C.P. No. 892

C.P. No. 892

MINISTRY OF AVIATION

AERONAUTICAL RESEARCH COUNCIL

CURRENT PAPERS

An Experimental Investigation of the Influence of Base Bleed on the Base Drag of Various Propelling Nozzle Configurations

By

J. B. Roberts and G. T. Golesworthy

(With an Appendix by W. G. E. Lewis and M. V. Herbert)

LONDON HER MAJESTY'S STATIONERY OFFICE

1966

Price 12s 6d net

U.D.C. No. 621-225.1 : 533.691.18.093 : 533.6.013.12

C.P. No.892*

February, 1964

An experimental investigation of the influence of base bleed on the base drag of various propelling nozzle configurations

- by -

J. B. Roberts and G. T. Golesworthy

SUMMARY

Various propelling nozzle configurations with all-internal expansion were tested in external flow over the range of Mach number 0.7 to 2.2, in order to determine the effect of base bleed (i.e. the injection of low energy secondary air) on base pressure. An 'overall efficiency' is defined, which enables the effectiveness of base bleed, as a means of reducing the base drag, to be assessed. The results indicate that with supersonic external flow base bleed generally tends to raise the level of base pressure, but no improvement in the overall efficiency is obtained. At subsonic external speeds, the secondary air has a negligible effect on base pressure.

*Replaces N.G.T.E. Report No. R.259 - A.R.C.26 228

CONTENTS

ILLUSTRATIONS

ILLUSTRATIONS

1.0 Introduction

For the engine installation of proposed supersonic transport aircraft, the exit area of an internal expansion, convergent-divergent propelling nozzle, such as would be appropriate to the exhaust pressure ratio at cruise, often proves to be considerably less than the cross-sectional area of the engine nacelle. A relatively large base area is thus created, and the problem arises of minimising the drag associated with it. Proposed methods of reducing this drag are summarised as follows:

(i) Base drag may be completely eliminated by extending the nozzle until its exit area coincides with the nacelle cross-sectional area. The nozzle flow will then be over-expanded at cruise, and the internal performance will suffer. At off-design conditions the penalty may be large.

(ii) The nacelle may be boat-tailed sufficiently to reduce the base area to zero, whilst retaining the correct nozzle exit area. Base drag is then replaced to some extent by boat-tail drag of the nacelle.

(iii) Base drag may be reduced by allowing a small quantity of low energy, secondary air to escape into the base region (this technique is known as base bleed or base ventilation). The exit area of the nozzle appropriate to cruise conditions may then be retained, or the nozzle may be shortened. It has been suggested that base bleed is more effective with such a shortened nozzle at cruise, and some improvement in internal nozzle performance at off-design conditions could be anticipated. Various combinations of base bleed and boat-tailing are also possible.

With the intention of helping to decide which of these systems offers the best solution, and more especially to investigate the effectiveness or otherwise of base bleed as a technique, a series of convergent-divergent model nozzles has been tested on cold dry air. These models were axisymmetric throughout, for convenience of manufacture and testing, although it should be remembered that for proposed supersonic transport aircraft the nacelle cross-section may be square or rectangular.

2.0 Description of test equipment

2.1 The external flow rig

A description of the external flow rig used for these tests will be found in Reference 1. The rig consisted of two alternative working sections, illustrated in Figure 1. Each line comprised a nozzle, viewing section and pressure recovery diffuser, the supply and exhaust arrangements being common to both lines. External flow from Mach number 0.7 to 1.5 could be provided by the upper or 'transonic' line, whilst the lower 'supersonic' line operated from Mach number 1.3 to 2.4. Test models were carried on a long parallel, hollow sting, which passed through the throat of the test line nozzles, and could be interchanged between them.

Figures 2 and 3 show the arrangement of the sting carrier section, which fitted immediately ahead of either external flow nozzle. This consisted of a round duct with a streamlined bullet carried on its centreline by a single hollow arm. From the bullet, the sting, with the model on its downstream end, was supported so that the outlet plane of the model was located in the window of the viewing section. Air, controlled

externally, was delivered to the model through the inner, load-carrying tube. The instrumentation and control lines from the model passed between the inner tube and the outer cover of the sting.

The transonic line was equipped with a slotted nozzle of circular cross-section, 11.3 inches in diameter (see Figure 2), the outlet Mach number of which could be varied simply by adjusting the applied pressure. A two-dimensional, flexible wall nozzle was used for the supersonic line, the nozzle outlet being 12 in. × 12 in. (see Figure 3).

2.2 Test models

All the various builds of model tested were founded on a common basic unit. A typical nozzle configuration built from this unit is shown in Figure 4.

The secondary or bleed flow was obtained by tapping off some of the primary nozzle flow, through vents upstream of the throat, and the amount tapped off was controlled by a remotely actuated ring valve, located in the annular secondary passageway between the inner and outer surfaces of the model. Secondary mass flow was estimated by passing the air through a constricted section downstream of the ring valve, equipped with pitot tubes and static tappings, as shown in Figure 4.

Parts additional to those in Figure 4 enabled various builds of model to be constructed. These builds formed modifications of two 'basic' designs, which are illustrated in Figure 5. Both have parallel outer shrouds, with coplanar exists, and area ratios of 2.050 and 2.789 (the corresponding design pressure ratios are 11.1 and 18.8 respectively).

Two modifications appear in Figure 6. Figure 6a shows a model incorporating some degree of external boat-tailing ($1^{\circ}30'$). In other respects, this build is identical to the 'basic' short nozzle, as in Figure 5a. Figure 6b shows the construction of a non-coplanar (or extended shroud) nozzle. This was formed by fitting the outer shroud of the 'basic' long nozzle (see Figure 5b) to the short primary nozzle of Figure 5a.

For some tests on the short nozzle, the base aperture was partly blocked. In one such arrangement, the bleed flow was discharged adjacent to the primary nozzle exit (see Figure 7a), whilst in another it passed on either side of the blocking piece (see Figure 7b).

3.0 Instrumentation and air supplies

The models were fitted with the following pressure instrumentation (the circled numbers in Figures 4 to 7 refer to the location of these tappings, and will be quoted where possible):-

(a) Two pitot and two static tubes situated in the primary nozzle inlet, upstream of the bleed flow take-off points (Numbers 1, 2, 3 and 4 in Figure 4).

(b) Two pitot tubes situated in the primary flow between the bleed take-off points and the nozzle throat (Numbers 5 and 6 in Figure 4).

(c) Three pitot tubes and three wall static tappings in the bleed airflow measuring section, downstream of the control ring valve (Numbers 7, 8, 9, 10, 11 and 12, respectively in Figure 4).

(d) A tapping in the primary nozzle base thickness (Number 15 in Figure 5a).

(e) A tapping outside the primary nozzle at its outlet, indicating the static pressure in the base region (Number 16 in Figure 5a).

(f) Two tappings inside the primary nozzle at its outlet, indicating the static pressure in the primary flow (Numbers 13 and 14 in Figure 5a).

(g) Either one or two tappings in the outer shroud base thickness (Number 17 in Figure 5a and Numbers 17 and 18 in Figure 5b).

(h) Either one or two tappings inside the shroud at its end, indicating the static pressure in this region (Number 19 in Figure 5a and Numbers 19 and 20 in Figure 5b).

(i) A tapping outside the shroud at its end (Number 21 in Figure 5a).

(j) Five tappings along the outside of the boat-tailed shroud (Numbers 24 to 28 in Figure 6a).

(k) In some builds, a reversed pitot tube in the base annulus (Number 22 in Figure 5a).

(l) In some builds, a pitot tube placed in the base flow passageway (Number 37 in Figure 5a).

(m) In the models with partial base blockage, of the types shown in Figure 7, two sets of three base tappings each inserted in the blocking piece (Numbers 29 to 34 in Figure 7a). Also, two tappings located in the constricted region where the bleed flow escaped (Numbers 35 and 36 in Figure 7b).

Secondary mass flow was estimated from the readings of the single pitot and static tappings located in each of three of the six measuring section ports (Figure 4). The averages of these readings were treated as mean total and static pressures acting over the constricted passage area, mass flow then being obtained according to one-dimensional isentropic relations. It is therefore likely that the values of secondary flow given here are over-estimated.

The height of the free-stream boundary layer at the nozzle exit plane was measured by attaching three pitot rakes (spaced circumferentially at 120°) to the end of the model. Their location is illustrated in Figure 8.

The temperature of the air supply to both model and test line nozzles was maintained within the range 25 to 35°C at all times. Air dryness was measured by an R.A.E.-Bedford pattern frost-point hygrometer, and held at better than -20°C frost-point throughout. Air supply pressure was at a level of 5 atmospheres and throttled independently as required for the model and external flow.

4.0 Model performance

A summary of the operating conditions of the various model builds is given in Table I.

4.1 Base pressure characteristics

The aim of all these tests was to examine, for each operating condition, the variation of base pressure with bleed mass flow. To obtain the results in a non-dimensional form, the conventional procedure is to plot $\frac{P_b}{P_\infty}$ against μ (see Appendix I for notation). In these tests μ is identical to the mass flow ratio, $\frac{Q_s}{Q_p}$, since the total temperature of the bleed air is equal to that of the primary flow.

Some caution is required when interpreting base pressure measurements. As mentioned in Section 3.0, a variety of pressure tappings was provided in the base region of these models. In many tests, particularly those on the short nozzle versions, these tappings indicated uniformity of base pressure for low quantities of bleed flow, the agreement steadily deteriorating as the bleed flow increased. A typical set of base pressure readings is presented in Figure 9 for the short nozzle with no boat-tailing and a coplanar exit, and Figure 10 gives a similar comparison for the long nozzle with coplanar exit. In the latter case, the spread at high bleed flow rates is much worse.

For the purposes of comparing model performance one with another, it is necessary to assume a single base pressure characteristic for each build. The base pressure results which follow have accordingly been obtained by averaging the available readings at each bleed flow value, despite the large differences occurring in some instances.

Before considering the experimental results in detail, some description will be given of the variations in flow pattern which are encountered.

The flow in the base region of a propelling nozzle with a coplanar exit is shown diagrammatically in Figure 11, for supersonic external flow and various operating pressure ratios. In Figure 11a we assume $\frac{P_b}{P_\infty} < 1$, so that the external stream expands around the lip of the outer shroud (at A). Also, in this example, the flow within the primary nozzle is under-expanded, and so continues to expand at the nozzle exit (at B) in a similar manner to the external stream. Clearly, the external and internal boundary layers (of thicknesses δ_E and δ_I respectively, as shown in Figure 11a) must detach at A and B, and free shear layers will develop in the regions A-C and B-C, dividing the stagnant base region from the supersonic streams on either side. At C, the two shear layers evidently converge in a recompression region.

If sufficient bleed flow is now injected to cause $\frac{P_b}{P_\infty}$ to exceed unity, the expansion at A is replaced by a shock, and the flow pattern is modified to Figure 11b.

Alternatively, if the pressure ratio across the nozzle is lowered, the expansion fan at B may be replaced by a shock, and the flow pattern will then be as Figure 11c. Further reduction in nozzle pressure ratio may cause the internal jet to separate from the walls, thus effectively increasing the width of the base. The appropriate flow pattern for the separated condition is shown in Figure 11d.

With subsonic external flow, the expansion fan or shock at A is replaced by a zone of gradual expansion or compression, and the recompression region at C may be expected to exhibit different characteristics.

Figure 12 presents the performance of the short nozzle with a coplanar exit, in supersonic external flow. The flow pattern here is evidently of the type depicted in Figure 11a. Small quantities of bleed flow (around 2 per cent of the primary mass flow) result in a significant increase in base pressure (some 40 per cent), but little further improvement is realised with higher quantities of bleed flow. For values of μ in excess of 5 per cent, the base pressure is sensibly constant. Figure 12 also indicates that a reduction in exhaust pressure ratio $\left(\text{E.P.R.} = \frac{P_t}{P_\infty}\right)$ causes a fall in the level of base pressure ratio.

The base pressure characteristics of the same nozzle in transonic and subsonic external flow are given in Figure 13, for values of E.P.R. appropriate to a supersonic transport aircraft operating at these flight conditions. In the case of $M_\infty = 1.1$ (Figure 13a), reduction of E.P.R. has resulted in an increase of base pressure level. This trend is clearly opposite to that observed in Figure 12, where the external Mach number and E.P.R. were higher. An effect of this nature is consistent with the results quoted in References 1 and 2, which indicate that, for a particular external Mach number, a critical value of E.P.R. exists at which the base pressure ratio is a minimum. When E.P.R. is reduced below this critical value, the base pressure ratio increases rapidly; above it the base pressure ratio rises slowly with increase of E.P.R. Reid and Hastings[2], working only at $M_\infty = 2.0$, attribute this discontinuity to a change of the recompression shock pattern in the external flow at C (Figure 11a), but Reference 1 shows a very similar behaviour of base pressure with change of E.P.R. in subsonic external flow.

A consideration of Reynolds number suggests that the primary nozzle boundary layer is turbulent throughout, for the conditions of these tests. At E.P.R. 4 in Figure 13a, the nozzle applied pressure ratio $\left(\text{A.P.R.} = \frac{P_t}{P_b}\right)$ varies from 5.8 to 5.0, and the nozzle should therefore be running full. This will, of course, also be true at any higher E.P.R. The flow pattern then resembles Figure 11c.

In the case of Figure 13b, relating to an external Mach number of 0.69, base pressure ratio is seen to be remarkably independent of both bleed flow rate and E.P.R., the general level of $\frac{P_b}{P_\infty}$ being around 0.9. The flatness of these curves is apparently associated with the presence of a subsonic external stream, a relation borne out by other results to

be mentioned later. Just the same effect has been obtained at O.N.E.R.A.[4], using a base bleed model very similar to that shown in Figure 5a, with an area ratio of about 2.6. Furthermore, recent theoretical work by Nash[3] does in fact predict that base bleed is likely to be ineffective in subsonic external flow at those values of Reynolds number.

Performance of the long model with a coplanar exit is presented in Figure 14, for external Mach Numbers of 2.2 and 1.8. These base pressure characteristics have a different shape to those discussed earlier, and the reason for this is not clear. However, the sense of variation of base pressure ratio with E.P.R. is similar to that observed in the short nozzle results. In Figure 15, the performance of this nozzle at subsonic speeds is given. Here again, the trends are similar to those observed for the short nozzle, and base bleed is clearly ineffective.

Shown for comparison on Figures 14 and 15 are some data extracted from Reference 1. The nozzle there had an area ratio of 2.90 (design pressure ratio 20) and a thin base, without bleed. It is interesting to note that, for the case of zero bleed flow, there is fairly close general agreement between the values of base pressure ratio obtained from Reference 1 and those from both 'basic' models in the present tests, despite quite large differences of design pressure ratio and base height (compare Figure 12a with 14a, 12b with 14b and 13b with 15b, for matching conditions of E.P.R.).

Now if the base region were able to be shielded from the external flow, it is reasonable to suppose that the benefits accruing from base bleed might be increased. This should be especially so in the case of a shortened primary nozzle at cruise conditions, where the internal static pressure in the exit plane is higher than ambient. To this end the extended shroud model of Figure 6b was tested.

Figure 16 depicts the flow pattern in the base region of the extended shroud system, for supersonic external flow and various nozzle operating conditions. In Figure 16a the operating pressure ratio is sufficient to cause the internal flow to expand at the primary nozzle exit (A). A free shear layer develops in the region A-B. Subsequently the jet reattaches on to the outer shroud at B, with accompanying recompression. At the same time, the free shear layer is rehabilitated on the shroud to form a new boundary layer. Finally, further expansion or compression will occur at C, depending upon overall conditions. Clearly, in this case, the base region is completely shielded from the external flow. So far as the internal flow is concerned, base pressure theory (e.g. Reference 5 relating to backward-facing steps) indicates that a reduction in E.P.R. may be expected to result in a proportional lowering of the base pressure ratio, the A.P.R. remaining constant for a given value of μ, provided always that the primary jet reattaches on the shroud. This is saying no more than that the region A-B-C in Figure 16a becomes effectively part of the internal expansion system, controlled only by the pressure at C.

Corresponding to Figure 16b would be the case when applied conditions are the same as for Figure 16a, but the shroud length is reduced so that reattachment cannot occur. The recompression zone will then lie outside the nozzle, and behaviour will be similar to that already described for the coplanar exit models.

At low values of A.P.R., the expansion at A is replaced by a shock which tends to deflect the internal flow away from the shroud, and will eventually prevent reattachment regardless of shroud length (Figure 16c). Still further reduction of A.P.R. gives Figure 16d, in which the internal flow is fully separated within the primary nozzle. In all these cases the external flow is able to influence conditions in the region A-C, so removing the immunity of base pressure to external flow enjoyed when reattachment takes place within the shroud.

At conditions when the external flow is subsonic, the internal situation will generally resemble that in Figure 16d, with no reattachment. The system is therefore likely to behave in a manner similar to the coplanar exit models, which were then insensitive to bleed flow.

It can be realised from the foregoing discussion that, for an extended shroud model to operate efficiently at cruise, the shroud should be long enough to permit internal reattachment. The critical length will depend upon the value of base pressure created in the region A-B (Figure 16a), which in turn is affected by the amount of bleed flow admitted.

The results of tests on the extended shroud model are presented in Figure 17, for supersonic external flow and various values of E.P.R. When $\frac{P_b}{P_{p,t}}$ is plotted against μ, the same results fall fairly close to a single curve (Figure 18), as would be expected if sufficient shroud length were available for reattachment to take place throughout the range of bleed flow.

For zero secondary mass flow, $\frac{P_b}{P_{p,t}} = 0.036$. If the internal flow is assumed to be inviscid, then once the Mach number at the primary nozzle exit is specified, the position of the jet boundary streamline may be calculated by the method of characteristics (in this case for axisymmetric flow). A computer programme[6] has been written for this purpose, and the result obtained when $\frac{P_b}{P_{p,t}} = 0.036$ is shown in Figure 19. In this computation, the outer shroud is assumed to be absent, and the boundary of the freely expanding jet is determined. The external shroud location is then superimposed on the drawing, to give an approximate indication of the minimum length for reattachment. Viscous effects will introduce some modification to the picture. At zero bleed flow, the shroud is of ample length. The corresponding flow pattern for $\frac{P_b}{P_{p,t}} = 0.085$ (corresponding to $\mu = 0.08$) appears in Figure 20. In this case, it will be observed that the outer shroud, no matter what its length, cannot contain an inviscid free-jet. However, in the presence of secondary flow, the reattachment streamline can no longer be assumed to coincide with the inviscid jet boundary. This could mean that the picture given by Figure 20 is to some extent pessimistic. The scatter of the experimental points in Figure 18 at higher bleed flows may be due to partial failure of the primary jet to reattach.

Values of base pressure ratio obtained with the extended shroud model in subsonic external flow are given in Figure 21. In their 'flat' character these curves resemble those for coplanar models, as previous consideration of the flow patterns suggested.

Test results for the boat-tailed model of Figure 6a are shown in Figures 22 and 23. Figure 22 is for M_∞ 2.2 and 1.8. These curves exhibit a maximum value of base pressure ratio at bleed flow rates varying between 4 and 6 per cent. The pronounced fall in the level of base pressure ratio at high bleed flows is thought to be due to the increased velocity at which the secondary air is discharged through the constricted base passage. Figure 23 relates to transonic and subsonic external flow, and comparison with Figure 13 for the 'basic' short nozzle shows little difference as a result of boat-tailing at these conditions.

Before any test data became available from other builds, some opinion held that the performance of the short nozzle with a coplanar exit might be improved by introducing partial blockage in the base region, and causing the bleed air to be discharged at high velocity. The models illustrated in Figure 7 were accordingly tested at M_∞ 2.2. Figure 24 indicates that the high injection velocity of the bleed air has in fact produced the opposite effect to that required. As can be seen, the base pressure ratio remains either almost independent of bleed flow, or actually falls with increasing flow.

In Figure 25 is presented a comparison at M_∞ 2.2 between the base pressure characteristics of all the model builds with a short primary nozzle. It is evident that the extended shroud model makes much the most effective use of bleed air. At low bleed flows, the boat-tailed build is superior to the 'basic' short nozzle, although inferior to the extended shroud. This advantage disappears at larger bleed flow, when the velocity of bleed discharge becomes too high. Still greater discharge velocities occurring in those models with partial base blockage are clearly detrimental.

It should be borne in mind that some further drag is associated with the boat-tail. This component is included in the overall thrust efficiency, to be discussed in the next Section, and was derived from pressures measured on the boat-tail surface.

A similar comparison is made in Figure 26 for three builds with a short primary nozzle at M_∞ 0.7. No significant differences can be detected.

To sum up the effects of geometry and bleed flow on base pressure ratio alone, without regard to the overall picture, it is apparent that:-

(i) Bleed flow can increase base pressure ratio in supersonic external flow, rapidly at first and subsequently more gradually, so long as discharge velocity is low.

(ii) Boat-tailing as a general principle offers some improvement in supersonic external flow, subject to (i) above.

(iii) An extended shroud, of length sufficient to allow reattachment of the primary jet, successfully shields the bleed discharge from a supersonic external stream, and permits much higher values of base pressure ratio to be attained for a given bleed flow. The effect is particularly marked at high bleed flow.

(iv) With subsonic external flow and appropriate primary nozzle operating conditions, the value of base pressure ratio is virtually constant regardless of bleed flow or geometry.

4.2 Overall efficiencies

To enable the performance of the various nozzle configurations to be compared directly, a form of 'overall efficiency' (η) has been employed. The expression for η is given in Appendix II. This enables base pressure characteristics in terms of $\frac{P_b}{P_\infty}$ versus μ to be converted into efficiency characteristics (i.e. η versus μ), which provide a true measure of the effectiveness of base bleed as a method of reducing base drag. It should be noted that in the derivation of the efficiency expression, it is assumed that the secondary air is captured at free-stream conditions, and its inlet momentum has been computed on this basis. This momentum term can be very important at high bleed flows.

It is unnecessary to convert all the base pressure data into efficiency characteristics, since it has already been seen that the base blockage modifications to the short nozzle proved unsatisfactory. Furthermore, it has been observed that the performance of the short nozzle is considerably improved when the outer shroud is extended, and so it only remains to compare the following configurations on an efficiency basis:-

(a) short nozzle with extended shroud,

(b) 'basic' long nozzle with coplanar exit,

(c) short nozzle with boat-tailed exterior.

In Figure 27, the overall efficiency of these three configurations is plotted against the bleed flow ratio μ for M_∞ 2.2 and E.P.R. 20. The corresponding characteristic for the 'basic' short nozzle with coplanar exit is included for comparison. These results reveal the following points of interest:-

(i) For both the 'basic' short nozzle with coplanar exit and the boat-tailed model, the inlet momentum of the secondary air becomes a dominant factor in the expression for η as bleed flow increases, which the rise of $\frac{P_b}{P_\infty}$ with μ is insufficient to offset. This causes η to fall as μ increases.

(ii) As the base pressure characteristics would lead one to expect, the efficiency of the extended shroud model is markedly better than that of the 'basic' short nozzle. In this case, the rapid increase of $\frac{P_b}{P_\infty}$ with μ at low bleed flows is sufficient to overcome the effect of the secondary inlet momentum and the efficiency increases slightly up to a value of $\mu \approx 0.02$, whereafter it falls. The maximum efficiency is, however, only marginally better than that at zero bleed.

(iii) The best efficiency is obtained with the 'basic' long nozzle and no bleed.

On Figure 27 is also shown a value of η obtained from Reference 1 for a nozzle of design pressure ratio 20, with a thin base and no bleed, operating at the same conditions. This nozzle had a value of overall area ratio (maximum cross-sectional area/throat area) of 3.06, as compared with 3.39 for the present models. It should be noted that the efficiency values quoted in Reference 1 ordinarily exclude the drag force on the annular base. For comparison with the overall efficiency used in the present tests (Appendix II), it is necessary to deduct the base drag term as given in Reference 1.

Similar comparisons to that in Figure 27 have been made for various values of E.P.R. and external Mach number. At supersonic external speeds, the trends are consistently as indicated in Figure 27.

It will be observed that the nozzle tested in Reference 1 has a higher efficiency at cruise conditions than any of the base bleed models considered in this report.

A typical comparison with subsonic external flow ($M_\infty = 0.70$, E.P.R. = 3) is shown in Figure 28. It will be observed that under these conditions, none of the models benefited from the introduction of base bleed, η consistently falling as μ is increased. A corresponding value of η obtained from Reference 1 is again included.

5.0 External boundary layer measurements

Theoretical work[5] indicates that the level of base pressure achieved in this type of experiment is influenced, to a great extent, by the thicknesses of the internal and external boundary layers. To provide a datum for the test results, it is therefore necessary to measure or estimate the appropriate boundary layer parameters.

No attempt was made here to take measurements of the internal boundary layer. A method of estimating boundary layer thickness in a propelling nozzle may be found in Appendix IV of Reference 7.

The external boundary layer in the model exit plane was explored by means of the pitot rake described in Section 2.2. Experimental velocity profiles were found to be independent of free-stream Mach number, and the results were therefore averaged. Velocity profiles obtained in the 12 in. × 12 in. supersonic line and the 11.3 in. transonic line are displayed in Figures 29 and 30 respectively, where they are compared with one-ninth and one-eleventh power law profiles. It will be observed that the experimental results do not conform to either of these power laws. The appropriate boundary layer thickness for the supersonic line was 0.80 in., whilst for the transonic line it was 0.62 in.

These values amount to 23 per cent and 18 per cent respectively of the overall model diameter. For comparison, the engine nacelle of a supersonic aircraft might be expected to grow a boundary layer around 12 per cent of its diameter by the nozzle outlet plane. For a given afterbody geometry, this implies that the ratio of boundary layer thickness to base height is unrepresentatively high in the present work. On the evidence of Reference 8, there is in consequence a general tendency to over-estimate base pressures.

By assuming that the total temperature throughout the boundary layer is constant, it is possible to calculate, for a given external Mach number, the displacement thickness (δ^*) and momentum thickness (θ) from the experimental velocity profile. Variation of these quantities with M_∞ is presented in Figures 31 and 32.

6.0 Conclusions

In most of the nozzle configurations which were tested, base bleed was observed to raise the level of the base pressure ratio, so long as the external flow was supersonic and the nozzle was running full. When the external flow was subsonic and appropriately low pressure ratios were applied to the nozzle, base bleed was found to be consistently ineffective.

On comparing the results in terms of an overall efficiency, and debiting the free-stream inlet momentum of the bleed air, it is found that no significant increase in efficiency can be obtained by employing base bleed in any of the configurations under any conditions. It would appear that base bleed does not afford a general method of improving the performance of a propelling nozzle installation.

There is definitely no case for cutting short the internal expansion surfaces of a nozzle in order to provide an area for introduction of base bleed. In the case of a long-range transport aircraft, better all-round nozzle performance can be obtained by continuing the primary expansion at least as far as is required to reach ambient pressure at cruise.

ACKNOWLEDGEMENTS

The authors wish to acknowledge the assistance given in this work by Mr. C. Overy, Miss M. Faiers and Miss V. Searle.

This experimental investigation was undertaken at the request of the British Aircraft Corporation, who designed and built the test models. The experimental work was carried out at the National Gas Turbine Establishment, and the results presented in this report have been independently assessed. Figures 4 to 8 have been taken from the relevant design drawings, with the kind permission of the British Aircraft Corporation.

REFERENCES

No.	Author(s)	Title, etc.
1	G. T. Golesworthy M. V. Herbert	The performance of a conical convergent-divergent nozzle with an area ratio of 2·9, in external flow. A.R.C. C.P.891 November, 1963
2	J. Reid R. C. Hastings	The effect of a central jet on the base pressure of a cylindrical afterbody in a supersonic stream. A.R.C. R. & M.3224 December, 1959
3	J. F. Nash	Private communication 1963
4	P. Carrière M. Sirieix	Unpublished work at O.N.E.R.A. Châtillon-sous Bagneux, France, 1963
5	J. F. Nash	An analysis of two-dimensional turbulent base flow, including the effect of the approaching boundary layer. A.R.C. R. & M.3344 July, 1962
6	J. B. Roberts	Unpublished work at N.G.T.E. 1963
7	M. V. Herbert D. L. Martlew	The design point performance of model internal expansion propelling nozzles, with area ratios up to 4. A.R.C. R. & M.3477 December, 1963
8	G. T. Golesworthy J. B. Roberts C. Overy	The performance of conical convergent-divergent nozzles of area ratios 2·44 and 2·14 in external flow. A.R.C. C.P.893 February, 1964

TABLE I

Nozzle operating conditions

Model build	Mach No.	Exhaust pressure ratios
Short nozzle with coplanar exit	2.20	20.44, 15.52
	1.80	14.92, 12.19
	1.10	7.01, 4.05
	0.69	5.66, 3.01
Long nozzle with coplanar exit	2.20	20.52, 18.45, 16.45
	1.80	14.72, 11.75
	0.89	6.02, 3.01
	0.70	5.07, 2.96
Short nozzle with extended shroud	2.20	20.01, 17.94, 15.94, 14.02
	2.01	19.96, 17.98, 15.97, 14.03
	0.88	6.06, 3.02
	0.70	5.06, 3.02
Short nozzle with boat-tailing	2.20	19.50, 17.84, 16.00, 13.95
	1.80	14.95, 12.00
	1.09	7.12, 3.97
	0.70	5.00, 3.00
Short nozzle with partial base blockage - type (a)	2.20	19.95, 17.95, 16.25, 14.40
Short nozzle with partial base blockage - type (b)	2.20	20.05, 17.95, 15.50, 14.02

APPENDIX I

Notation

A	cross-sectional area
D	drag force
F	thrust force
K	flow parameter $\left(= \frac{Q\sqrt{T_t}}{A^* P_t} \right)$
M	Mach number
P	pressure (static unless otherwise stated)
Q	mass flow
R	gas constant for air (= 96 ft lb/lb°K)
T	temperature (static unless otherwise stated)
v	velocity
α	primary nozzle divergence half-angle
β	afterbody boat-tail angle
δ	boundary layer thickness
δ^*	boundary layer displacement thickness
θ	boundary layer momentum thickness
η	overall thrust efficiency of nozzle and bleed system (see Appendix II)
η_p	primary nozzle internal gross thrust efficiency
η_s	bleed air momentum efficiency
μ	bleed mass flow ratio $\left(= \frac{Q_s\sqrt{T_{s,t}}}{Q_p\sqrt{T_{p,t}}} \right)$

A.P.R. Applied pressure ratio = $\frac{\text{Primary nozzle entry total pressure}}{\text{Base pressure}}$

$$= \frac{P_{p,t}}{P_b}$$

E.P.R. Exhaust pressure ratio = $\frac{\text{Primary nozzle entry total pressure}}{\text{Ambient pressure}}$

$$= \frac{P_{p,t}}{P_\infty}$$

APPENDIX I (cont'd)

Suffices etc.

*	isentropic conditions in primary nozzle throat
b	base
e	primary nozzle exit
m	maximum cross-section of nacelle
n	cross-section of nacelle at exit plane
p	primary nozzle flow
s	secondary or bleed flow
t	total head conditions
B.T	boat-tail
∞	ambient conditions

APPENDIX II

The overall thrust efficiency of a propelling nozzle with base bleed

- by -

W. G. E. Lewis and M. V. Herbert

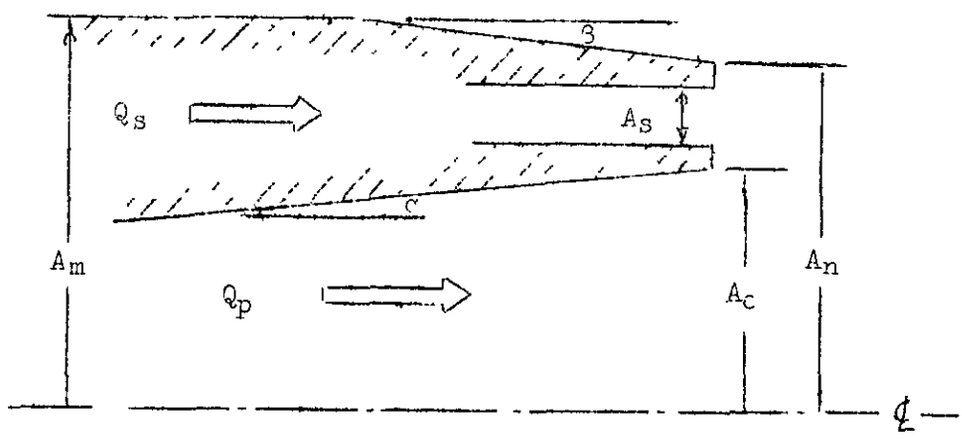

Case A. Conical primary nozzle running full.

We shall define the following force terms:-

F_p = momentum + pressure thrust of primary air at primary nozzle outlet

$$= \eta_{p,max} \cdot \frac{Q_p v_e}{g} + A_c(P_e - P_\infty) \qquad \ldots\ldots(1)$$

F_s = momentum of bleed air at outlet + base pressure thrust

$$= \eta_s \cdot \frac{Q_s v_s}{g} + (A_n - A_e)\ (P_b - P_\infty) \qquad \ldots\ldots(2)$$

D_s = inlet momentum of bleed air, assumed to be taken from free stream

$$= \frac{Q_s v_\infty}{g} \qquad \ldots\ldots(3)$$

$D_{B.T}$ = boat-tail drag of nacelle afterbody

$$= (A_m - A_n)\ (P_\infty - P_{B.T}) \qquad \ldots\ldots(4)$$

the signs being taken such that

$$\text{Total force} = F_p + F_s - D_s - D_{B.T}$$

We further define

$$F_{p,ideal} = \frac{Q_p v_{is}}{g}$$

where v_{is} is the fully-expanded isentropic velocity corresponding to

$$\frac{P_{p,t}}{P_\infty} \quad (= \text{E.P.R.})$$

The overall efficiency is given by

$$\eta = \frac{F_p + F_s - D_s - D_{B.T}}{F_{p,ideal}}$$

It is convenient to express all force quantities non-dimensionally in the form

$$\frac{F_{p,ideal}}{A^* P_{p,t}} = \frac{K_p}{g} \cdot \frac{v_{is}}{\sqrt{T_{p,t}}} \qquad \ldots\ldots (5)$$

where $K_p = \dfrac{Q_p \sqrt{T_{p,t}}}{A^* P_{p,t}}$

$$\frac{F_p}{A^* P_{p,t}} = \eta_{p,max} \cdot \frac{K_p}{g} \cdot \frac{v_e}{\sqrt{T_{p,t}}} + \frac{A_e}{A^*}\left(\frac{1}{\text{D.P.R.}} - \frac{1}{\text{E.P.R.}}\right) \qquad \ldots\ldots (6)$$

where
- v_e is the isentropic velocity corresponding to primary nozzle area ratio $\dfrac{A_e}{A^*}\left(\dfrac{2}{1 + \cos\alpha}\right)$
- D.P.R. is the primary nozzle design pressure ratio = $\dfrac{P_{p,t}}{P_c}$
- $\eta_{p,max}$ is the design-point efficiency of the primary nozzle

Now $$v_s = \frac{Q_s R T_s}{A_s P_b}$$

and putting $\mu = \frac{Q_s\sqrt{T_{s,t}}}{Q_p\sqrt{T_{p,t}}}$

we get $$\frac{Q_s v_s}{g} = \frac{\mu^2 K_p^2 R}{g} \cdot \frac{\left(A^* P_{p,t}\right)^2}{A_s P_b} \cdot \frac{T_s}{T_{s,t}}$$

$$\therefore \quad \frac{F_s}{A^* P_{p,t}} = \eta_s \cdot \frac{\mu^2 K_p^2 R}{g} \cdot \frac{A^*}{A_s} \cdot \left(\text{A.P.R.}\right) \cdot \frac{T_s}{T_{s,t}} + \left(\frac{A_n - A_e}{A^*}\right)\left(\frac{1}{\text{A.P.R.}} - \frac{1}{\text{E.P.R.}}\right) \qquad \ldots\ldots(7)$$

$$\frac{D_s}{A^* P_{p,t}} = \frac{\mu K_p}{g} \cdot \frac{v_\infty}{\sqrt{T_{s,t}}} \qquad \ldots\ldots(8)$$

$$\frac{D_{B.T}}{A^* P_{p,t}} = \left(\frac{A_m - A_n}{A^*}\right)\left(\frac{1}{\text{E.P.R.}} - \frac{P_{B.T}}{P_{p,t}}\right) \qquad \ldots\ldots(9)$$

Then η is evaluated as $\dfrac{(6) + (7) - (8) - (9)}{(5)}$

Notes

1. $P_{B.T}$ may be determined approximately for a given boat-tail angle β by using the appropriate two-dimensional Prandtl-Meyer relation, or from experimental pressure measurements if available.

2. In the present tests γ for all three streams can be taken as 1.4, so that $K_p = 0.3966$.

3. In (7) and (8) it will usually be possible to write $T_{s,t} = T_{\infty,t}$. In these particular tests it is true to put $T_{p,t} = T_{s,t} = T_{\infty,t}$.

4. In many cases it will be sufficiently accurate to take $T_s/T_{s,t} \simeq 1$ in (7), the first term of which amounts to a very small part of the whole force. For the same reason η_s is also taken to be unity in the absence of other information.

5. If the velocity of bleed air discharge is sufficiently great for the approximation in Note 4 to be unjustified, the value of $T_s/T_{s,t}$ can be found as follows:-

$$M_s^2 = \frac{\mu^2 K_p^2 R}{\gamma_s g} \cdot \left(\frac{A^*}{A_s}\right)^2 \cdot \left(\frac{P_{p,t}}{P_b}\right)^2 \cdot \frac{T_s}{T_{s,t}}$$

while $\frac{T_{s,t}}{T_s} = 1 + \frac{\gamma_s - 1}{2} M_s^2$

Hence $\frac{T_{s,t}}{T_s}\left(\frac{T_{s,t}}{T_s} - 1\right) = \frac{(\gamma_s - 1)}{2\gamma_s} \cdot \frac{\mu^2 K_p^2 R}{g}\left(\frac{A^*}{A_s}\right)^2 (A.P.R.)^2$

6. The value of primary nozzle design-point efficiency $\eta_{p,max}$ depends on D.P.R. and cone angle α. It may either be calculated approximately or derived from static thrust calibrations. For the primary nozzles of these tests, with $\alpha = 10^\circ$ and D.P.R. values 11.12 and 18.78, a figure of 0.988 was estimated from Reference 7 as appropriate to these test conditions.

7. If the primary nozzle should be other than conical, e.g. two-dimensional, the same relations are applicable except as regards the terms $\eta_{p,max}$ and $\frac{2}{1 + \cos\alpha}$.

Case B. Conical primary nozzle with internal separation.

Relations (2), (3), (4), (5), (7), (8), and (9) remain as in Case A, and Notes 1 to 5 apply. Alternative treatment must, however, be used for the quantity F_p when the primary nozzle is no longer running full. We will now write

$$F_p = \eta_p\left[\frac{Q_p v}{g}\right]_{APR} + A_e(P_b - P_\infty)$$

or $$\frac{F_p}{A^* P_{p,t}} = \eta_p \cdot \frac{K_p}{g}\left[\frac{v}{\sqrt{T_{p,t}}}\right]_{APR} + \frac{A_e}{A^*}\left(\frac{1}{A.P.R.} - \frac{1}{E.P.R.}\right) \quad .... (10)$$

where $\left[\frac{v}{\sqrt{T_{p,t}}}\right]_{APR}$ is the isentropic velocity term corresponding

to $\frac{P_{p,t}}{P_b}$ (= A.P.R.)

and η_p is the internal efficiency measured for the primary nozzle operating under static conditions at this value of A.P.R.

Then η is evaluated as $\frac{(10) + (7) - (8) - (9)}{(5)}$

Notes

8. To take an example, appropriate to curve 2 of Figure 28, for which

$$M_\infty = 0.7; \quad \text{E.P.R.} = 3; \quad \text{D.P.R.} = 11.12$$

we see from Figure 13 that $P_b/P_\infty \simeq 0.9$, giving A.P.R. = 3.33. At this condition a suitable value of η_p would be 0.92 with turbulent boundary layer separation.

9. It is worth observing that any primary nozzle of similar geometry but different D.P.R., provided that turbulent separation still occurs at the same A.P.R., will have a value of η_p at that condition quite close to that given in Note 8 above. This fact may be understood by reference to the sketch below, drawn for a particular A.P.R.

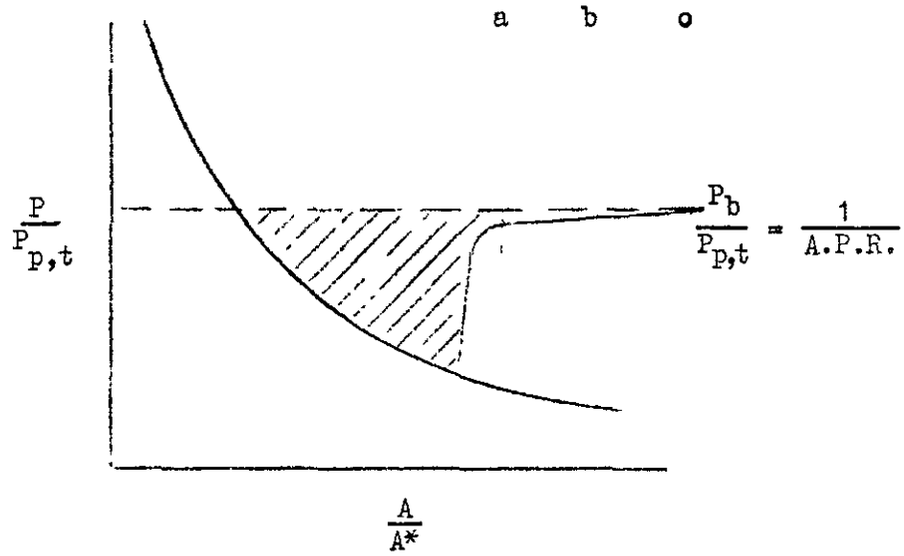

Due to the nature of the pressure rise occurring in a nozzle with turbulent boundary-layer separation, most of which is concentrated at the separation point as depicted, it will make very little difference to the internal performance, as represented by the shaded area, whether the nozzle ends at station a, b or c. For instance, at the condition of A.P.R. 3.33 with a turbulent boundary layer mentioned in Note 8, a 10° nozzle of D.P.R. 20 has $\eta_p \simeq 0{\cdot}90$ (Refs. 1 and 7), as compared with the value 0·92 taken for D.P.R. 11.12. It is therefore generally unnecessary for work of the present nature to carry out static thrust calibrations for every nozzle of different D.P.R. encountered.

10. In the special case of no bleed flow ($\mu = 0$) and no boat-tail ($\beta = 0$), the expression for overall efficiency reduces to

$$\eta = \frac{\eta_p \cdot \frac{K_p}{g}\left[\frac{v}{\sqrt{T_{p,t}}}\right]_{APR} + \frac{A_n}{A^*}\left(\frac{1}{\text{A.P.R.}} - \frac{1}{\text{E.P.R.}}\right)}{\frac{K_p}{g}\left[\frac{v}{\sqrt{T_{p,t}}}\right]_{EPR}}$$

It may be noted that, with the further condition of $A_n = A_e$ (zero base thickness), this reduces to the familiar symmetrical relation for single-stream nozzle internal performance

$$\eta_{F(EPR)} \frac{K}{g}\left[\frac{v}{\sqrt{T_t}}\right]_{EPR} + \frac{A_e}{A^*} \cdot \frac{1}{E.P.R.} = \eta_{F(APR)} \frac{K}{g}\left[\frac{v}{\sqrt{T_t}}\right]_{APR} + \frac{A_e}{A^*} \cdot \frac{1}{A.P.R.}$$

in which the notation is now as used, for instance, in Reference 1.

FIG.1

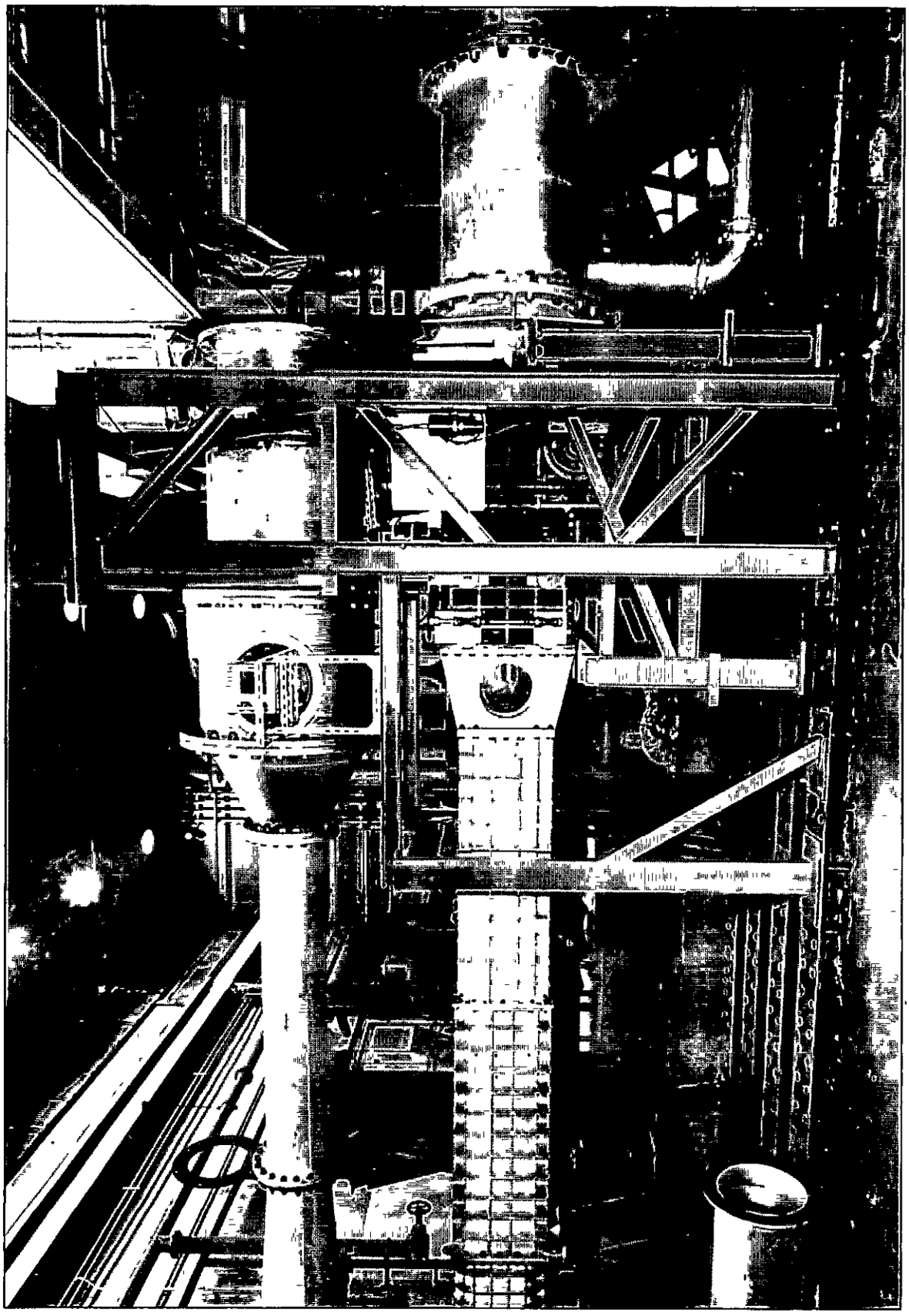

MODEL PROPELLING NOZZLE TEST RIG.

FIG. 2

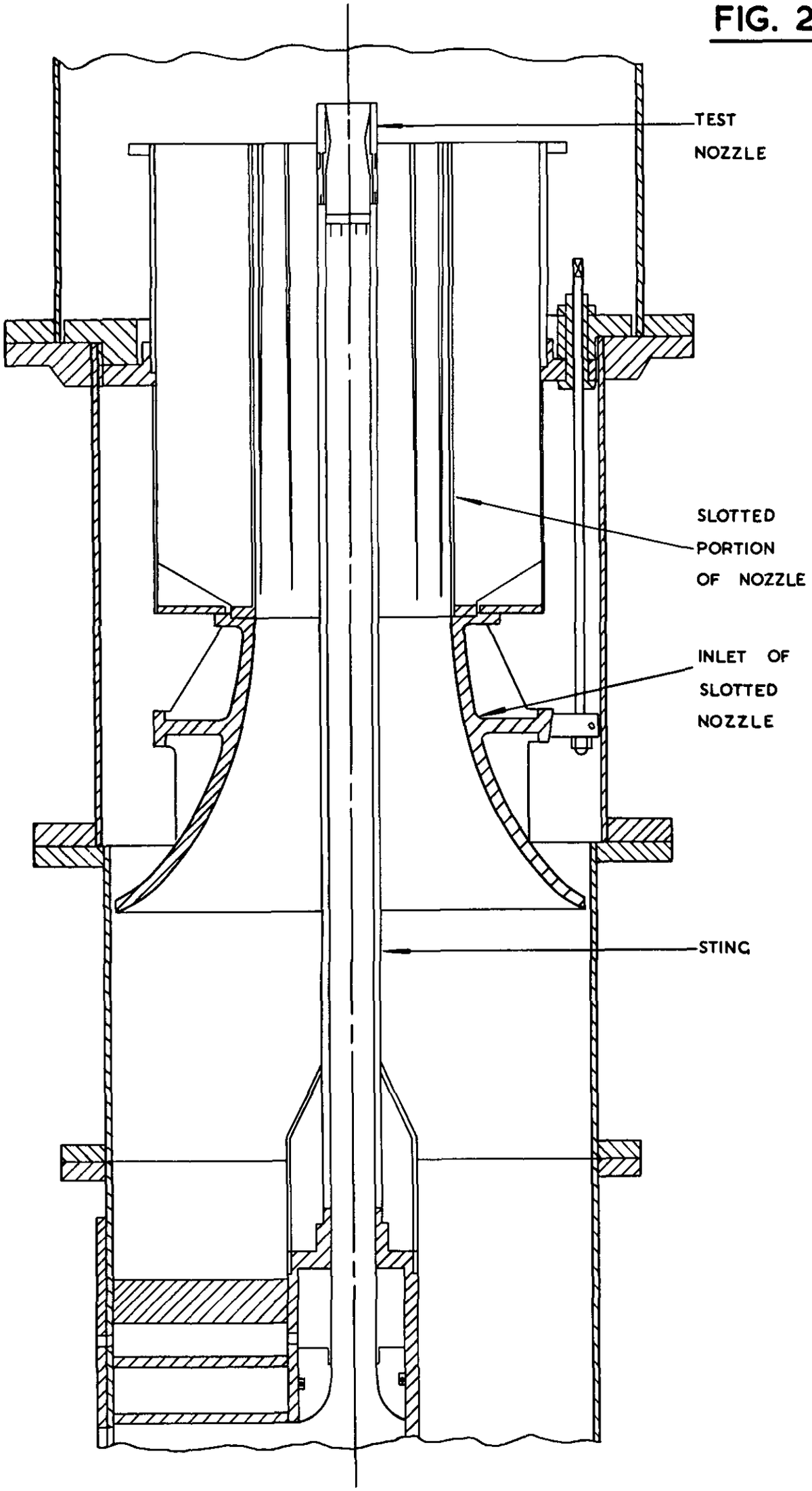

STING CARRIER SECTION IN TRANSONIC LINE.

FIG. 3

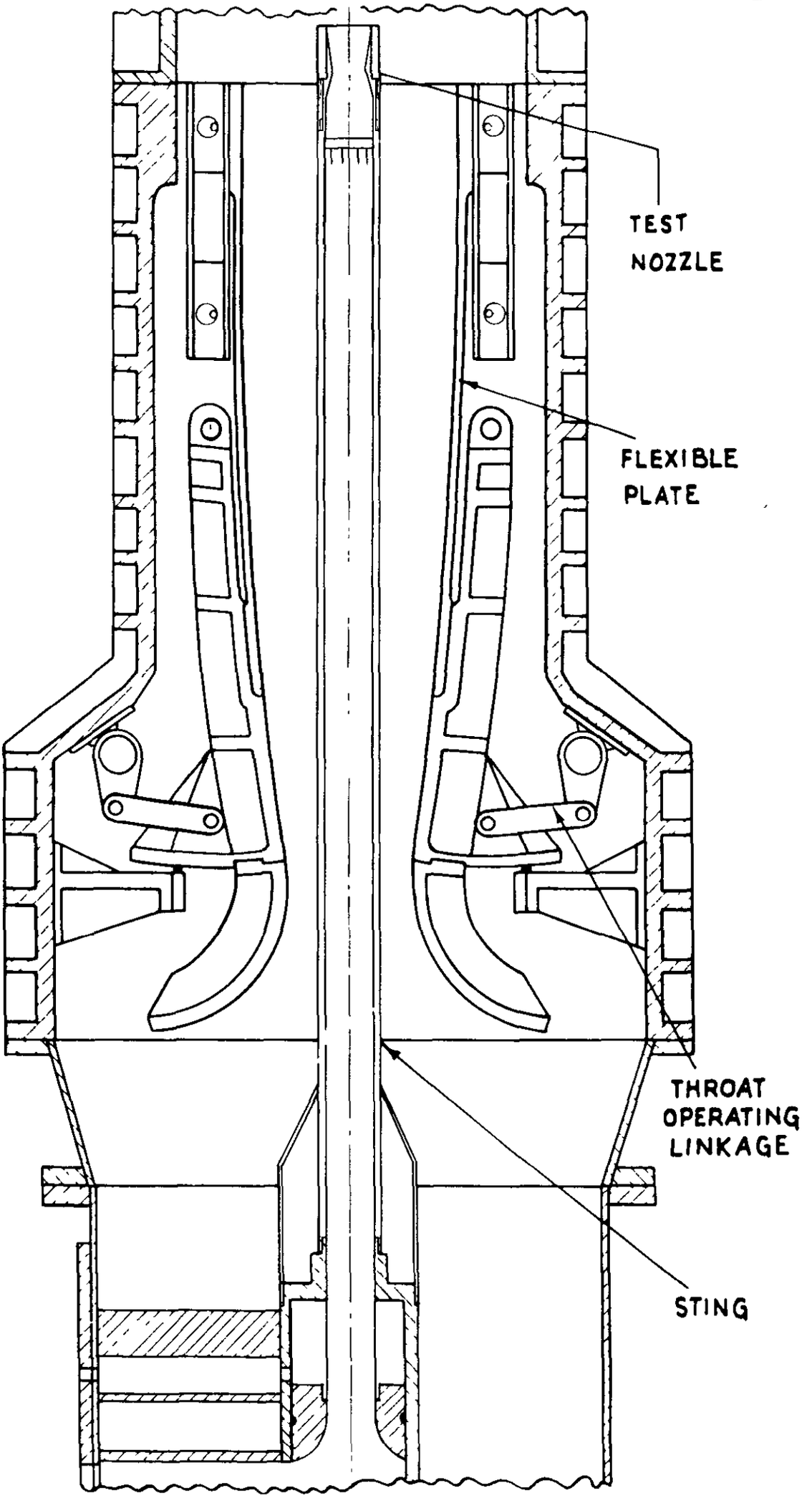

STING CARRIER SECTION IN SUPERSONIC LINE.

FIG. 4

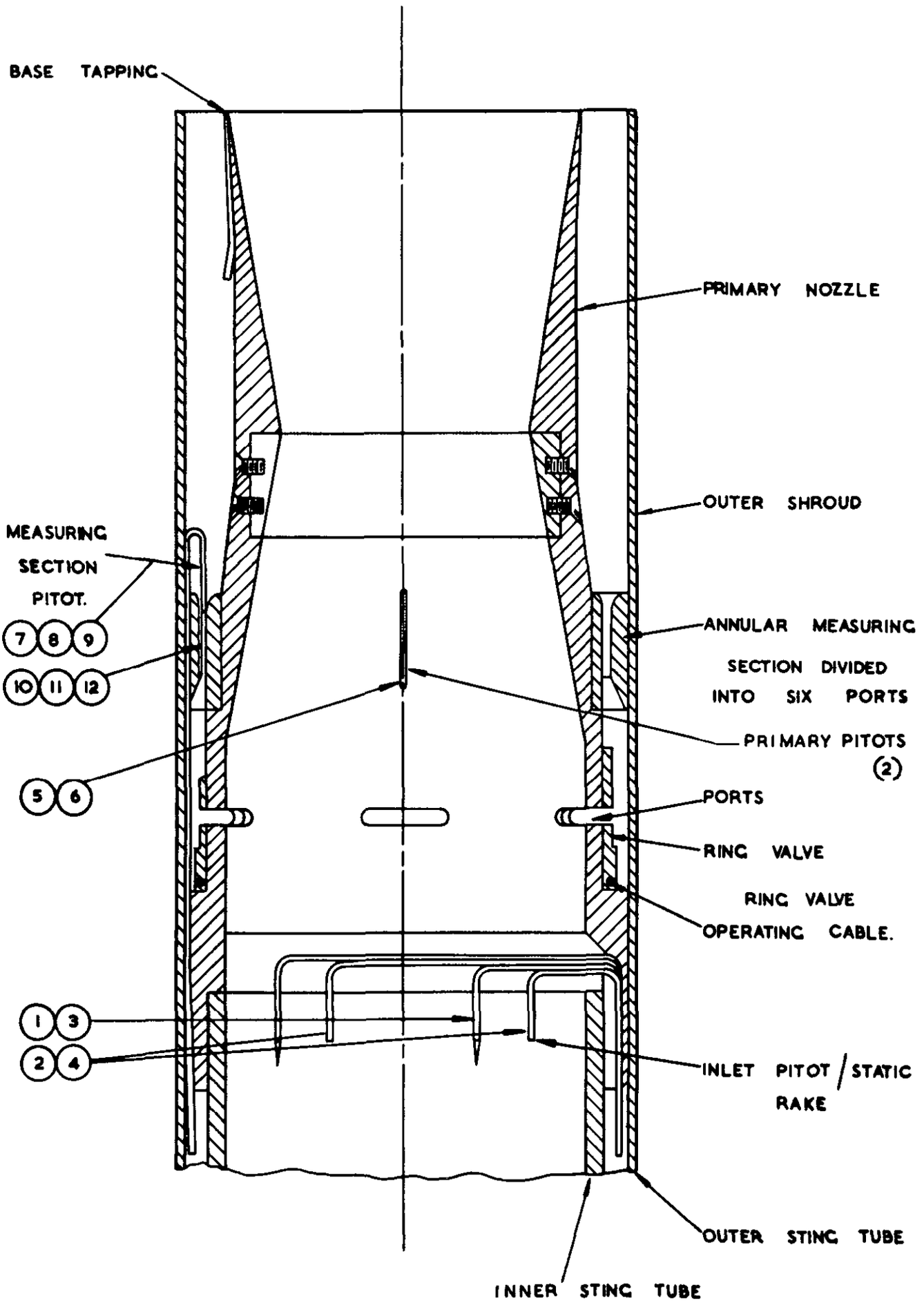

GENERAL CONSTRUCTION OF TEST NOZZLE.

FIG. 5.(a & b.)

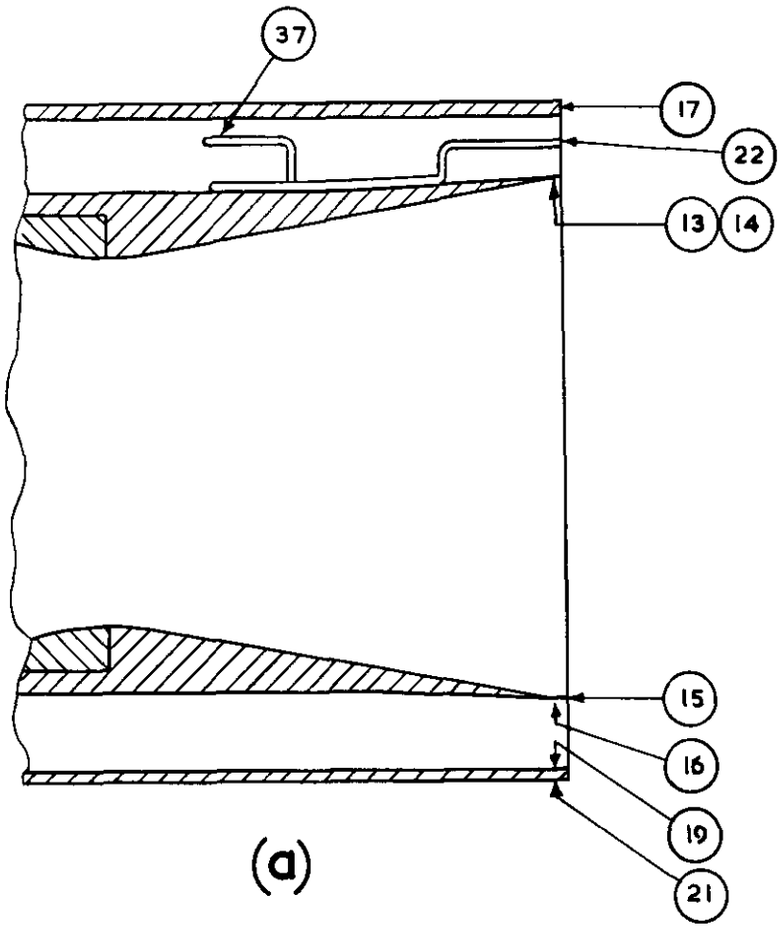

(a)

THROAT DIA. 1·90
PRIMARY EXIT DIA. 2·720
SHROUD OUTSIDE DIA 3 510

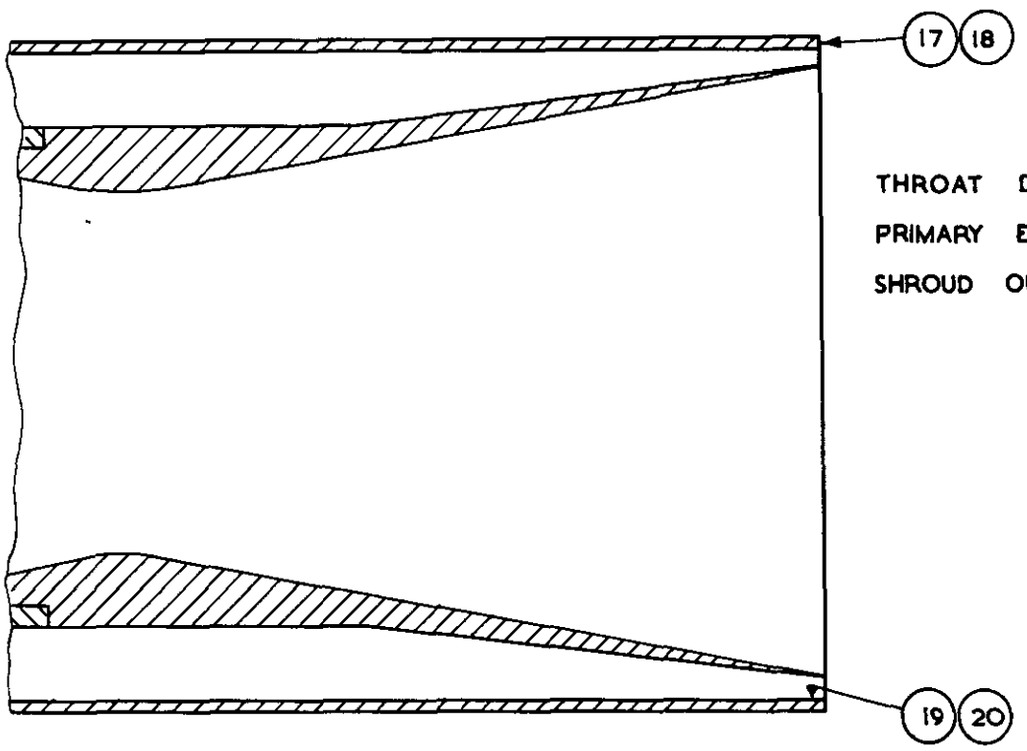

(b)

THROAT DIA 1·90
PRIMARY EXIT DIA 3 172
SHROUD OUTSIDE DIA. 3·510

GEOMETRY OF SHORT & LONG COPLANAR MODELS

FIG.6 (a & b.)

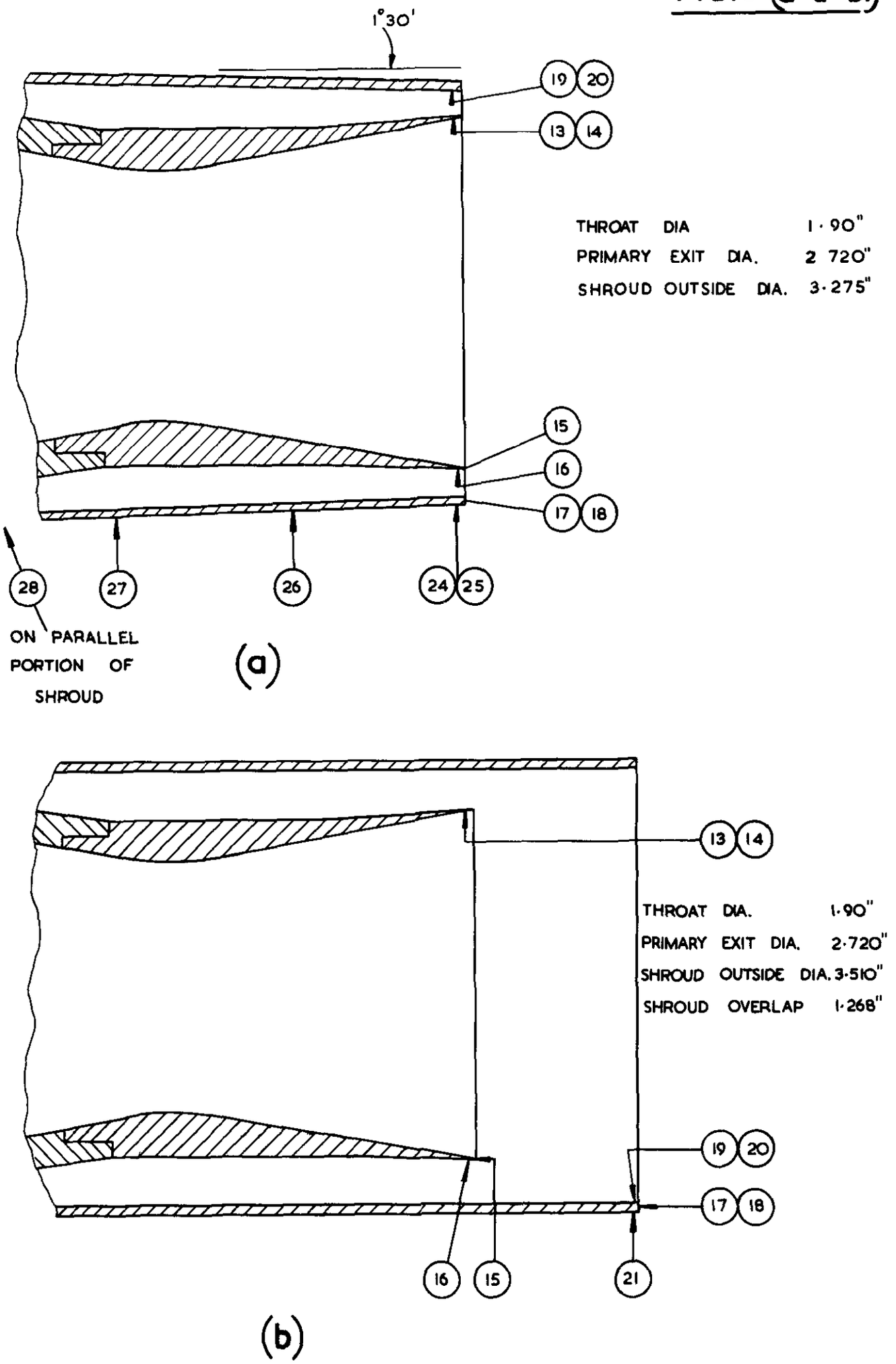

GEOMETRY OF EXTENDED SHROUD & BOAT-TAIL MODELS

FIG.7(a & b.)

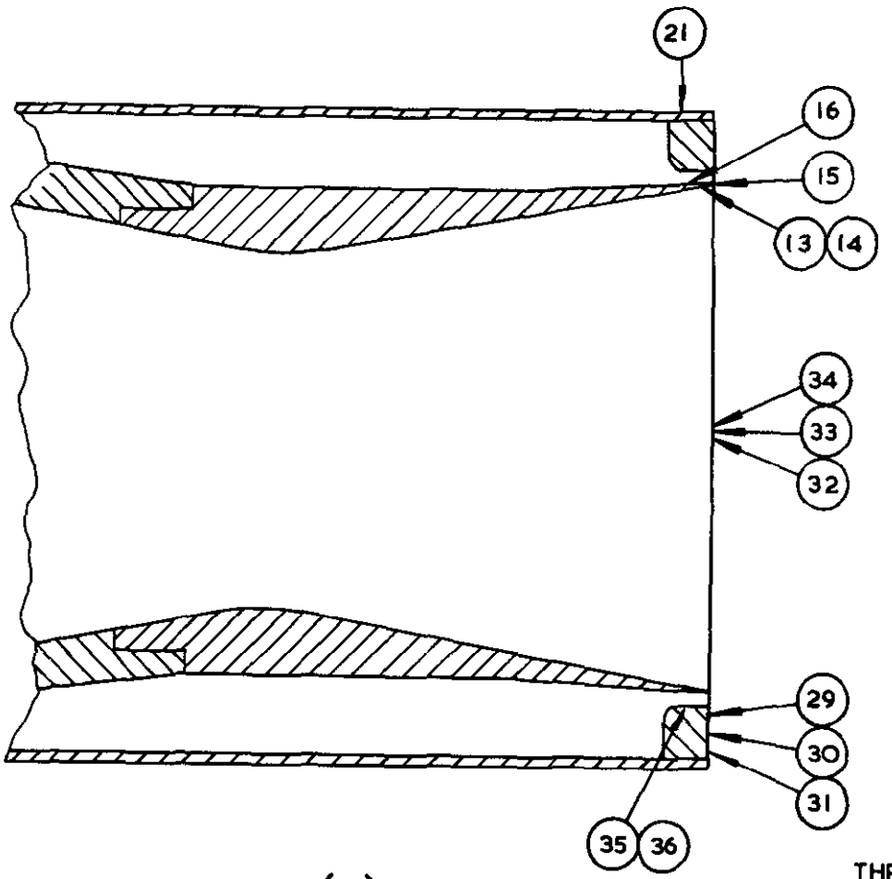

(a)

THROAT DIA 1·90"
PRIMARY EXIT DIA 2·720"
SHROUD OUTSIDE DIA 3·510"

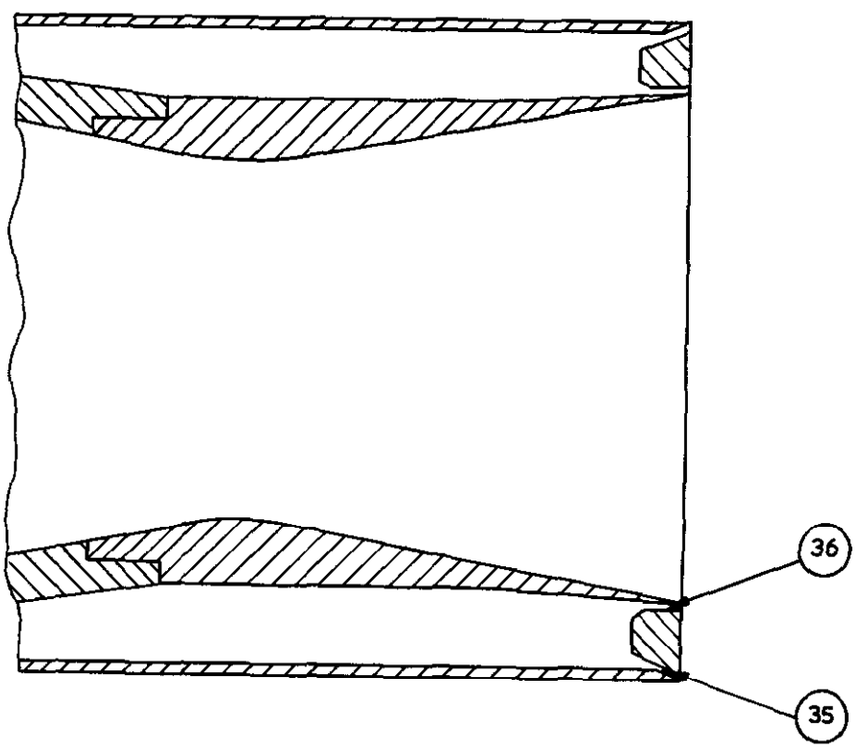

(b)

GEOMETRY OF BASE BLOCKAGE MODELS.

FIG. 8

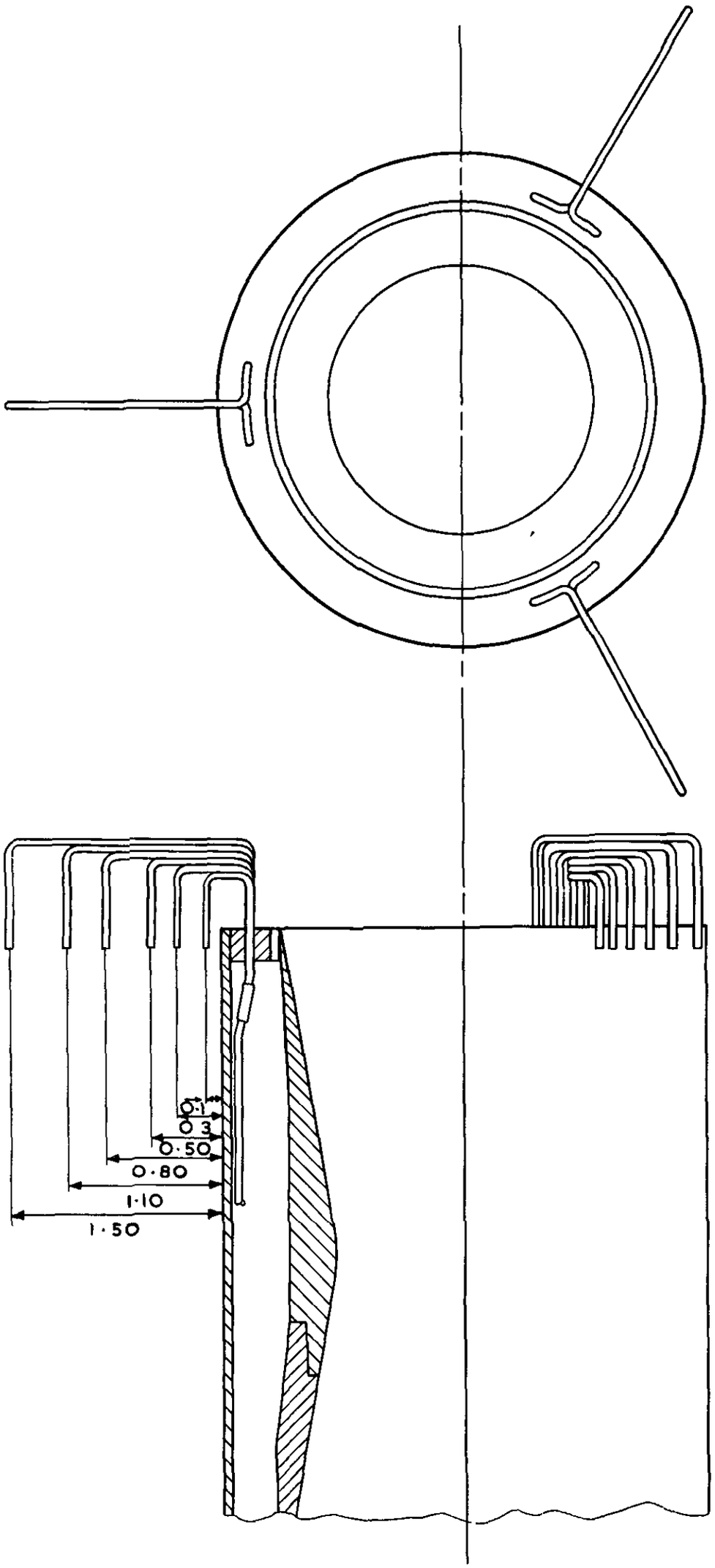

LOCATION OF PITOT RAKES
FOR BOUNDARY LAYER SURVEY

FIG. 9

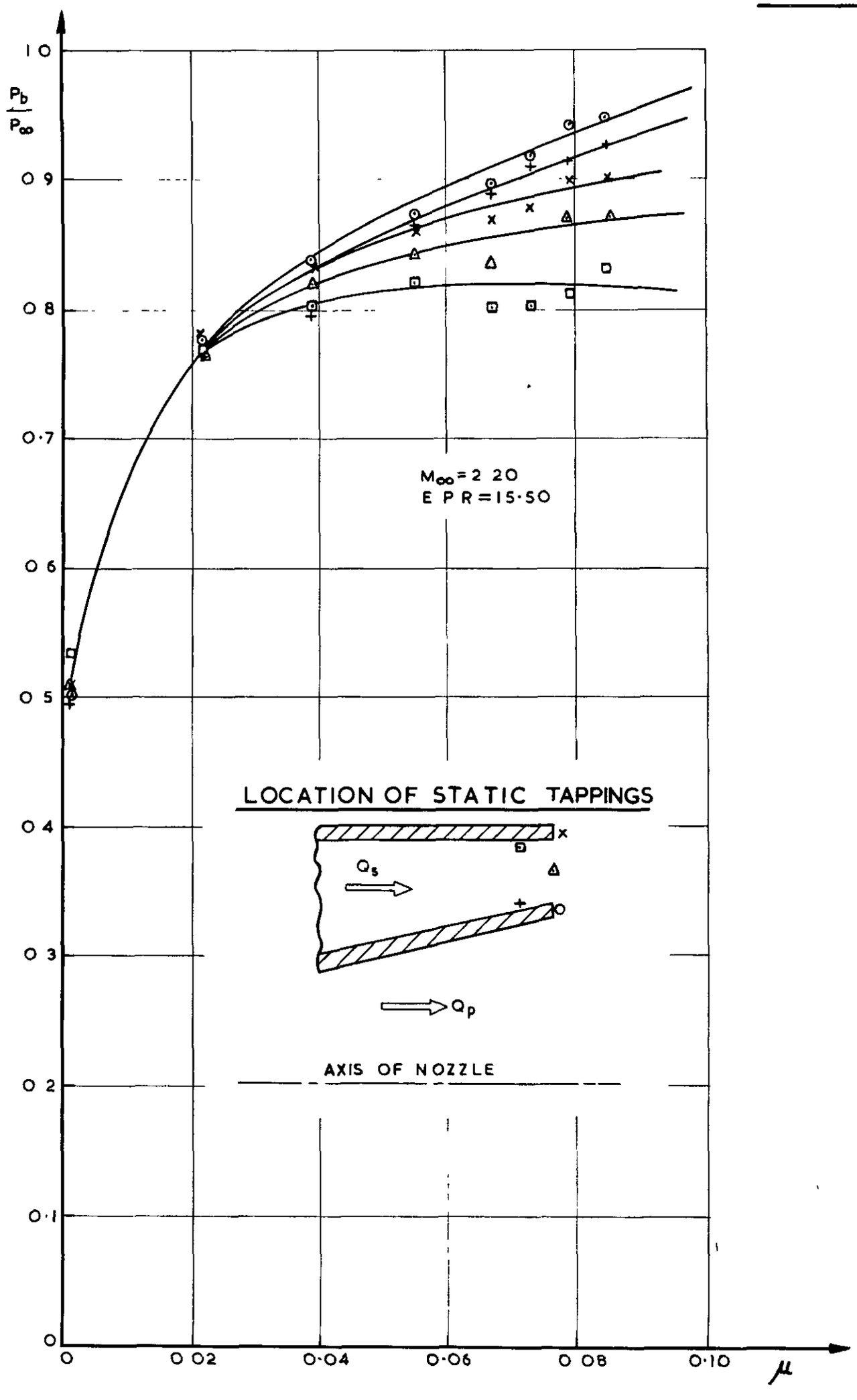

A COMPARISON OF BASE PRESSURE READINGS FOR SHORT NOZZLE WITH COPLANAR EXIT.

FIG. 10

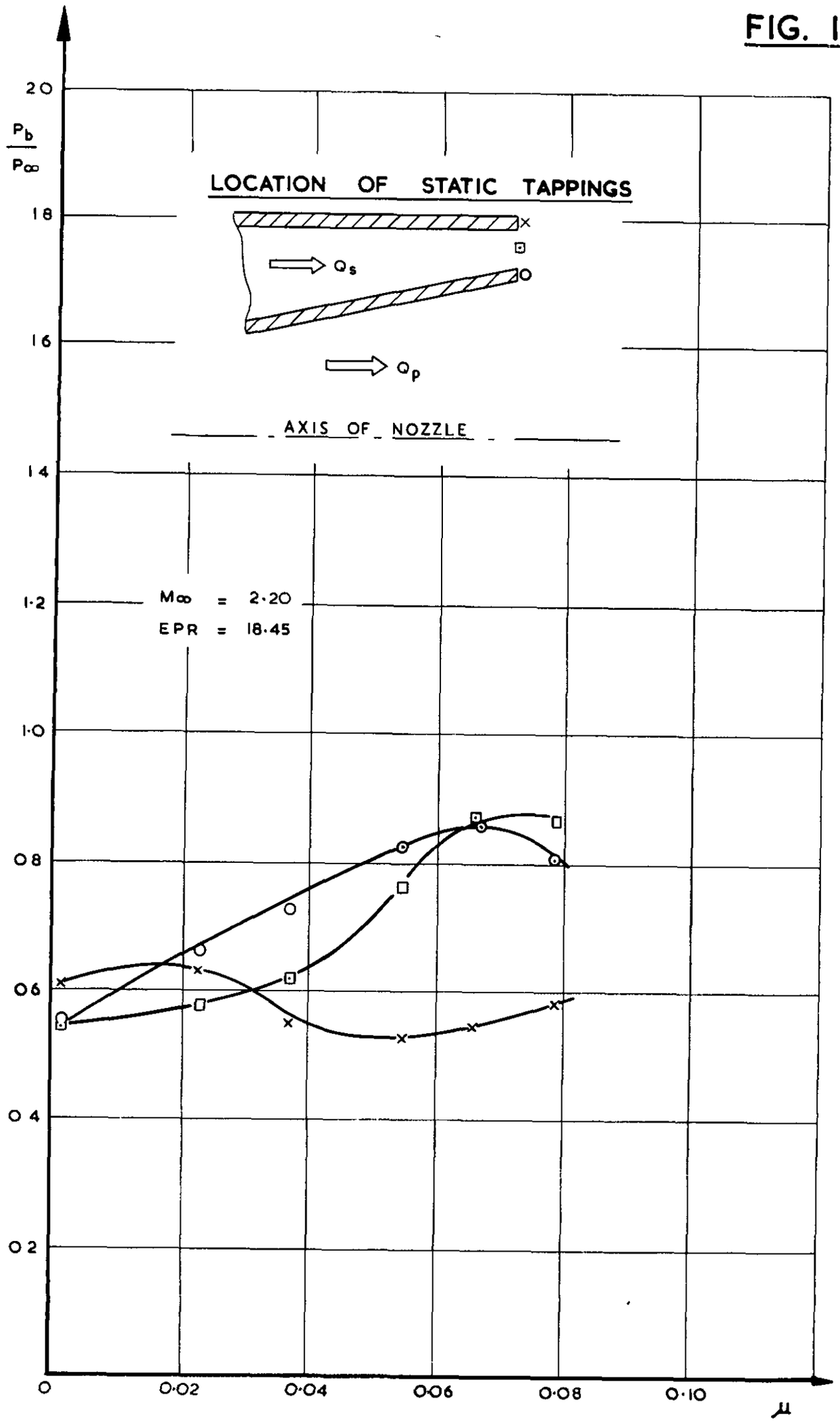

A COMPARISION OF BASE PRESSURE READINGS FOR LONG NOZZLE WITH COPLANAR EXIT.

FIG.11.

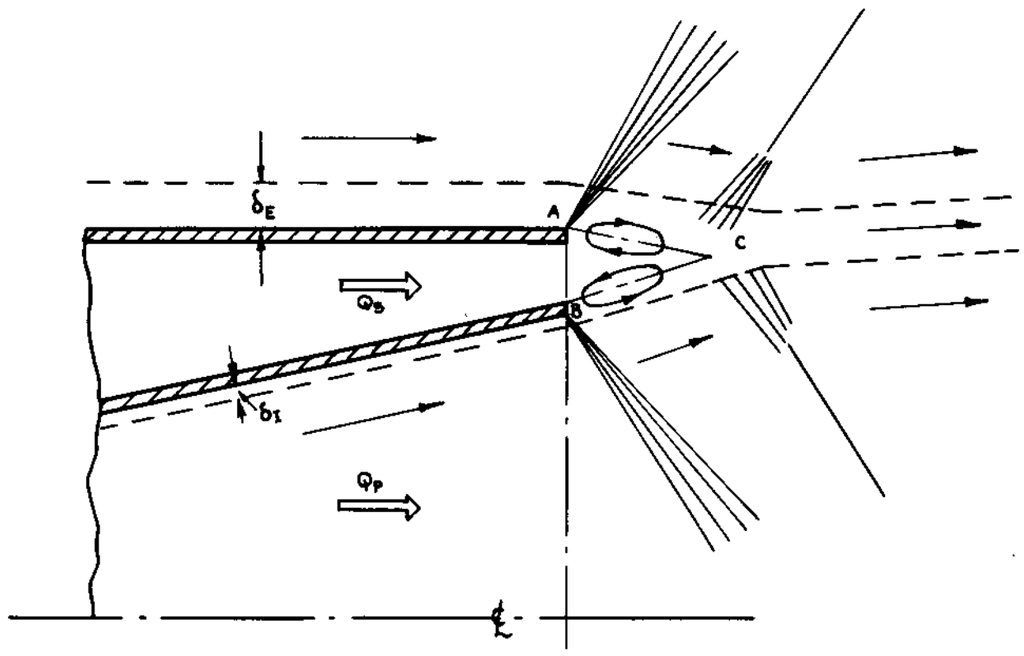

(a)

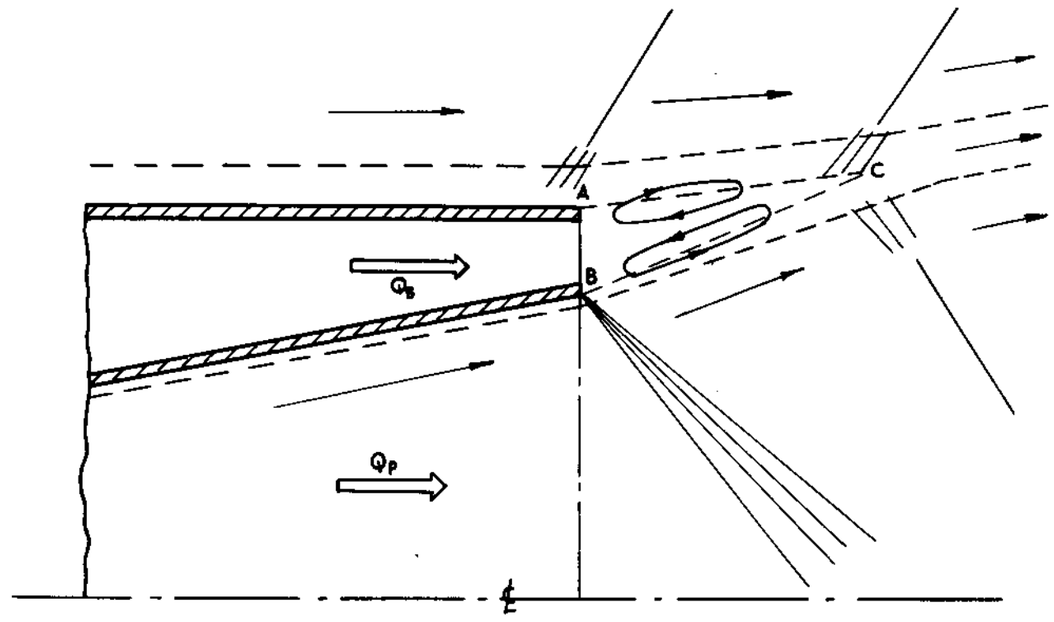

(b)

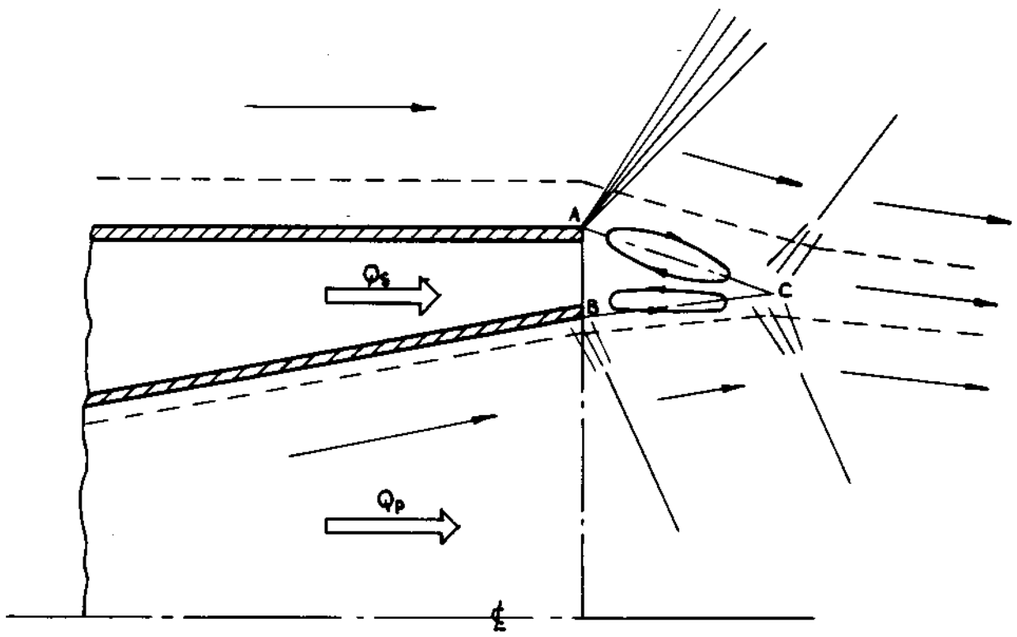

(c)

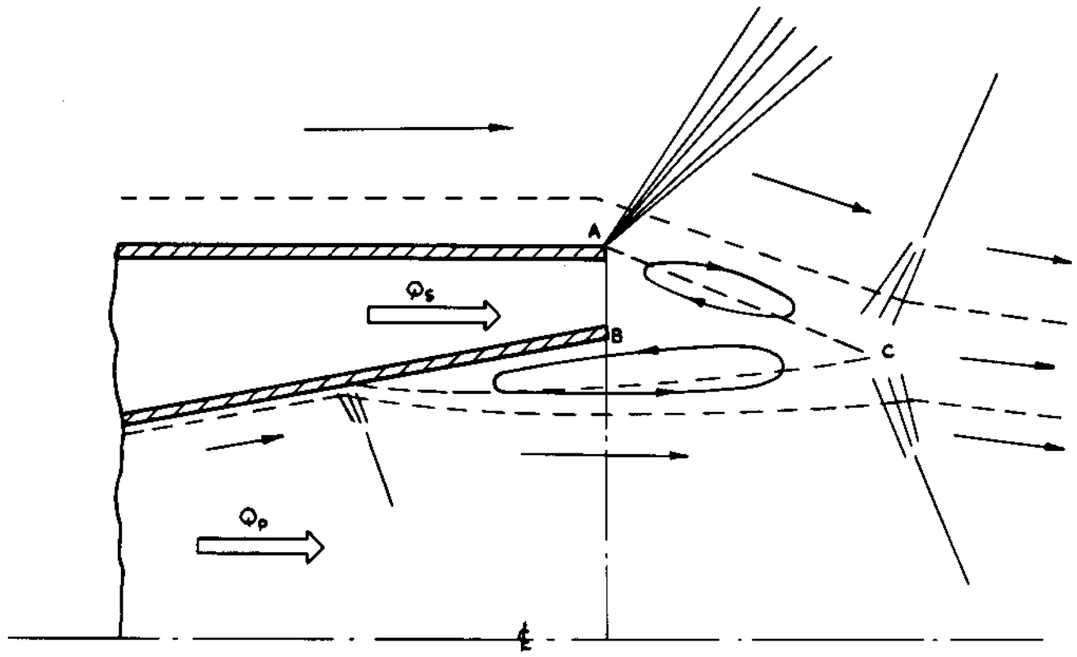

(d)

BASE FLOW PATTERNS FOR A NOZZLE WITH A COPLANAR EXIT, OPERATING IN EXTERNAL FLOW

FIG. 12 (a & b)

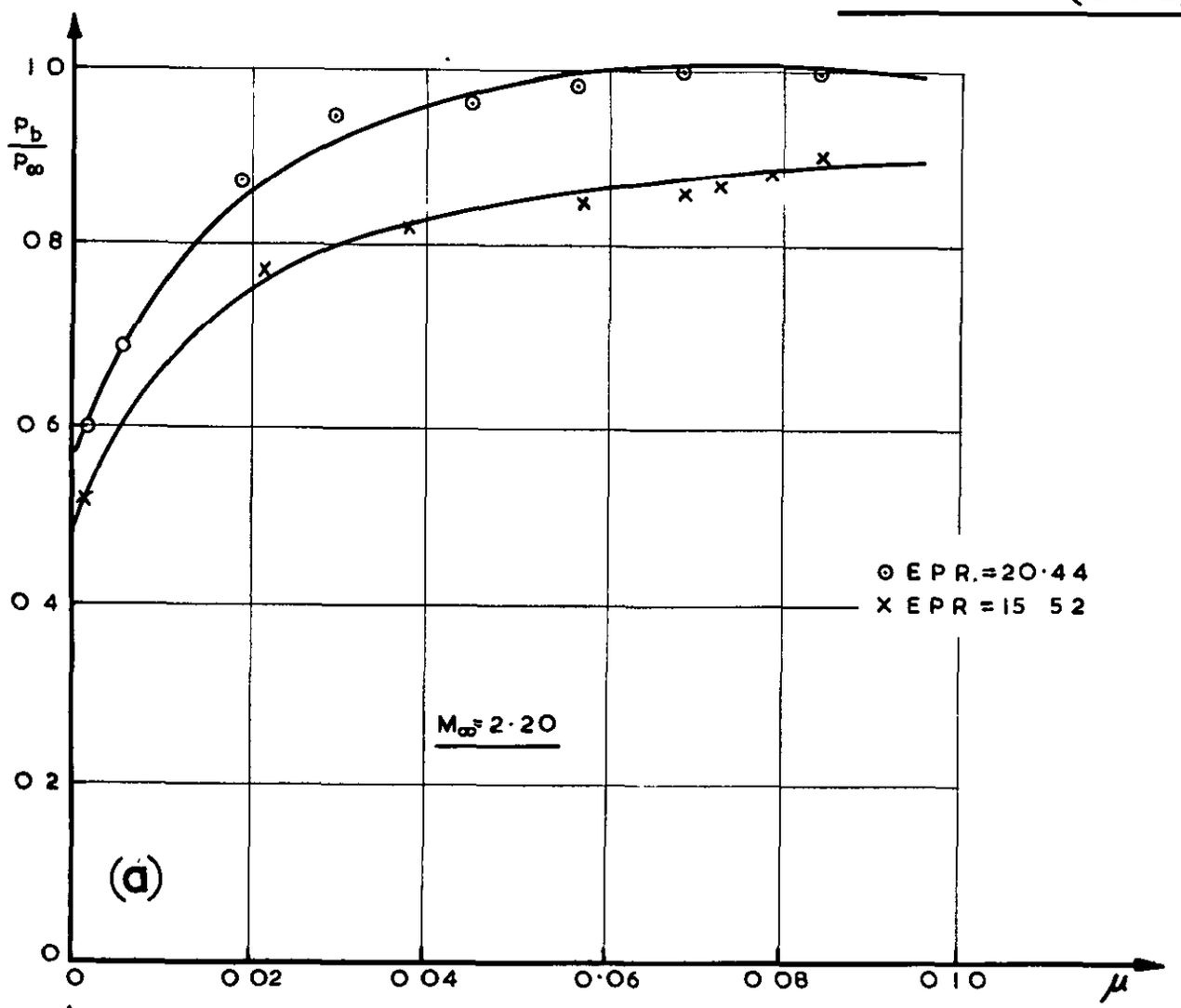

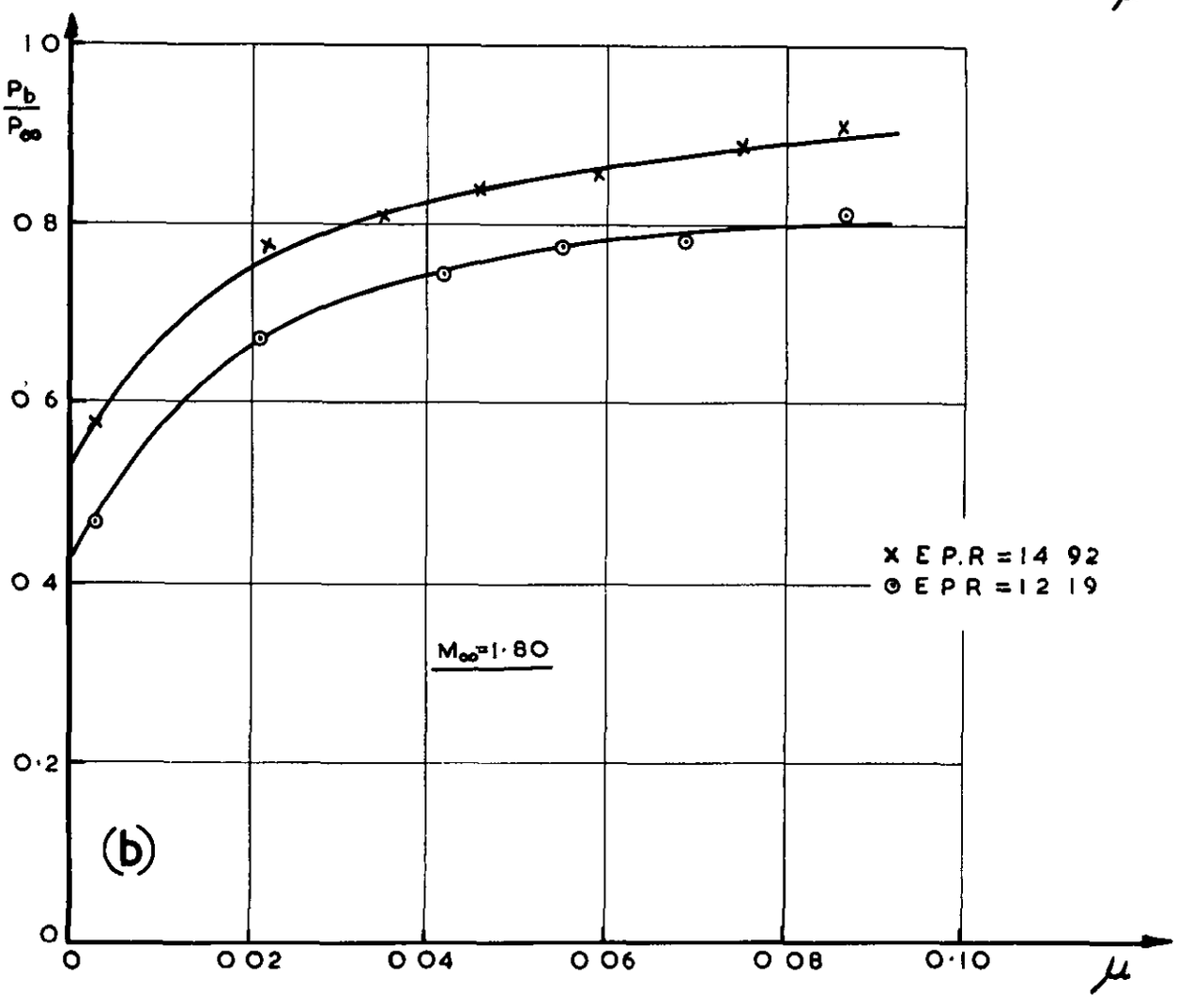

PERFORMANCE OF SHORT NOZZLE WITH COPLANAR EXIT.

FIG. 13 (a & b)

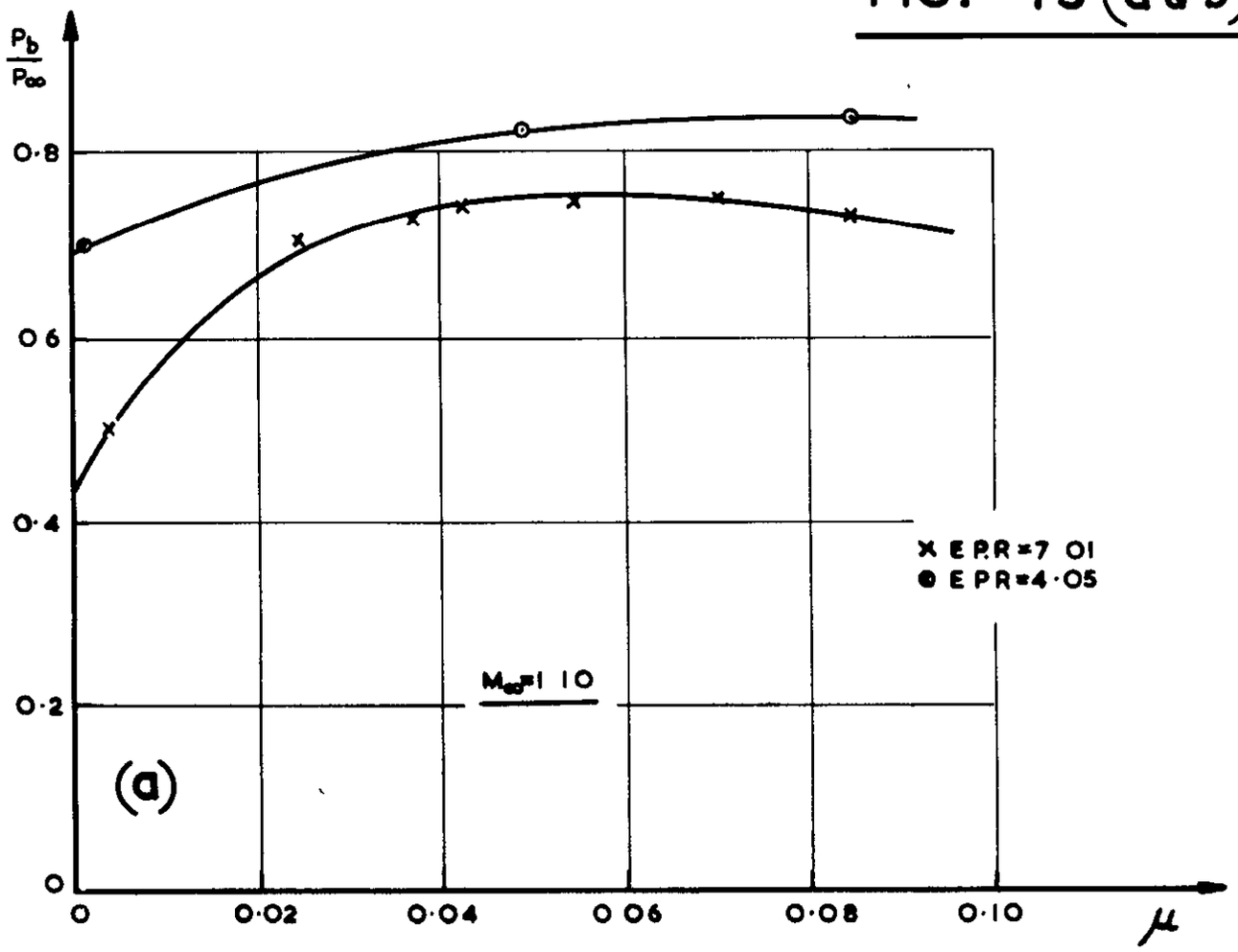

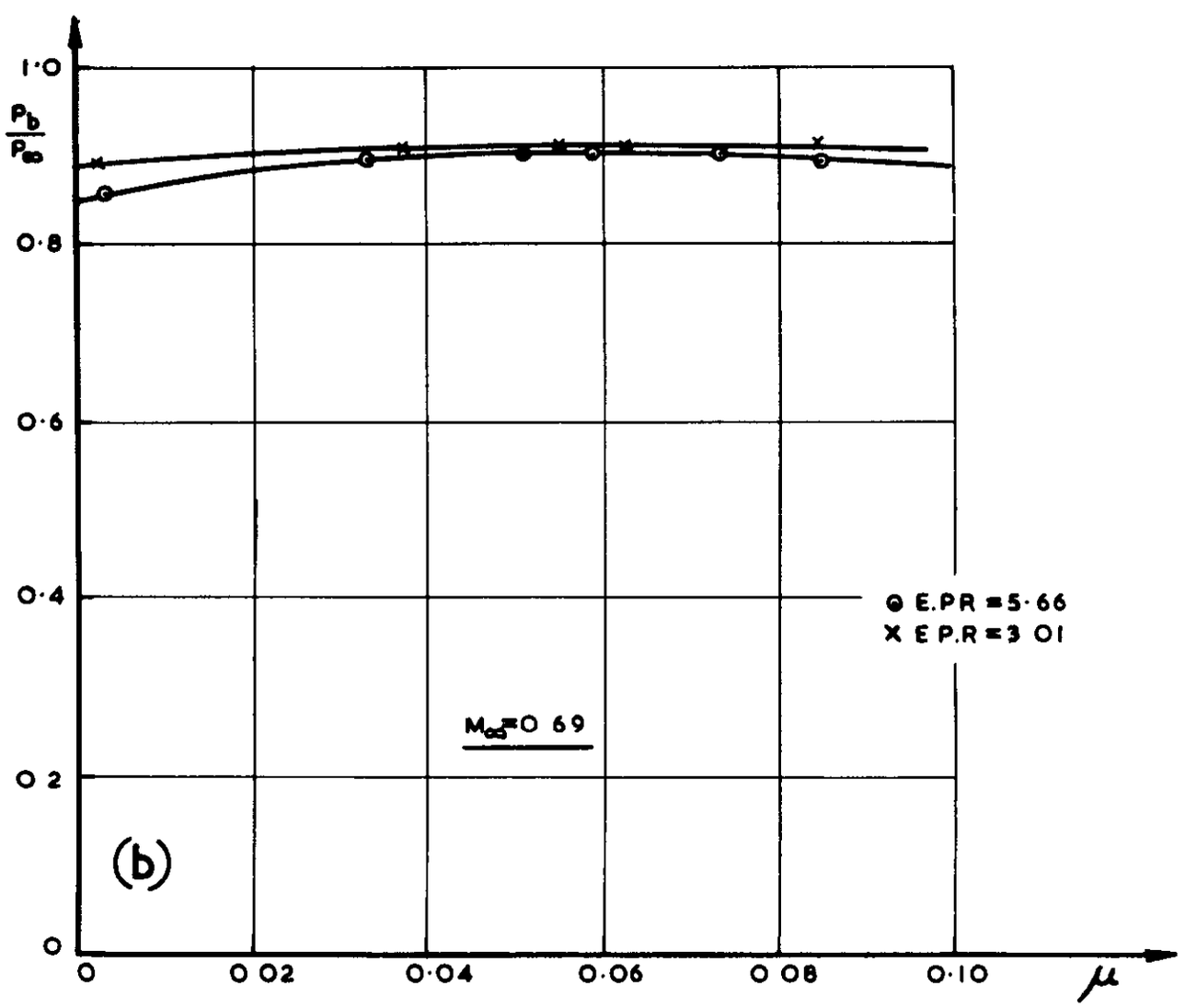

PERFORMANCE OF SHORT NOZZLE WITH COPLANAR EXIT.

FIG. 14 (a & b)

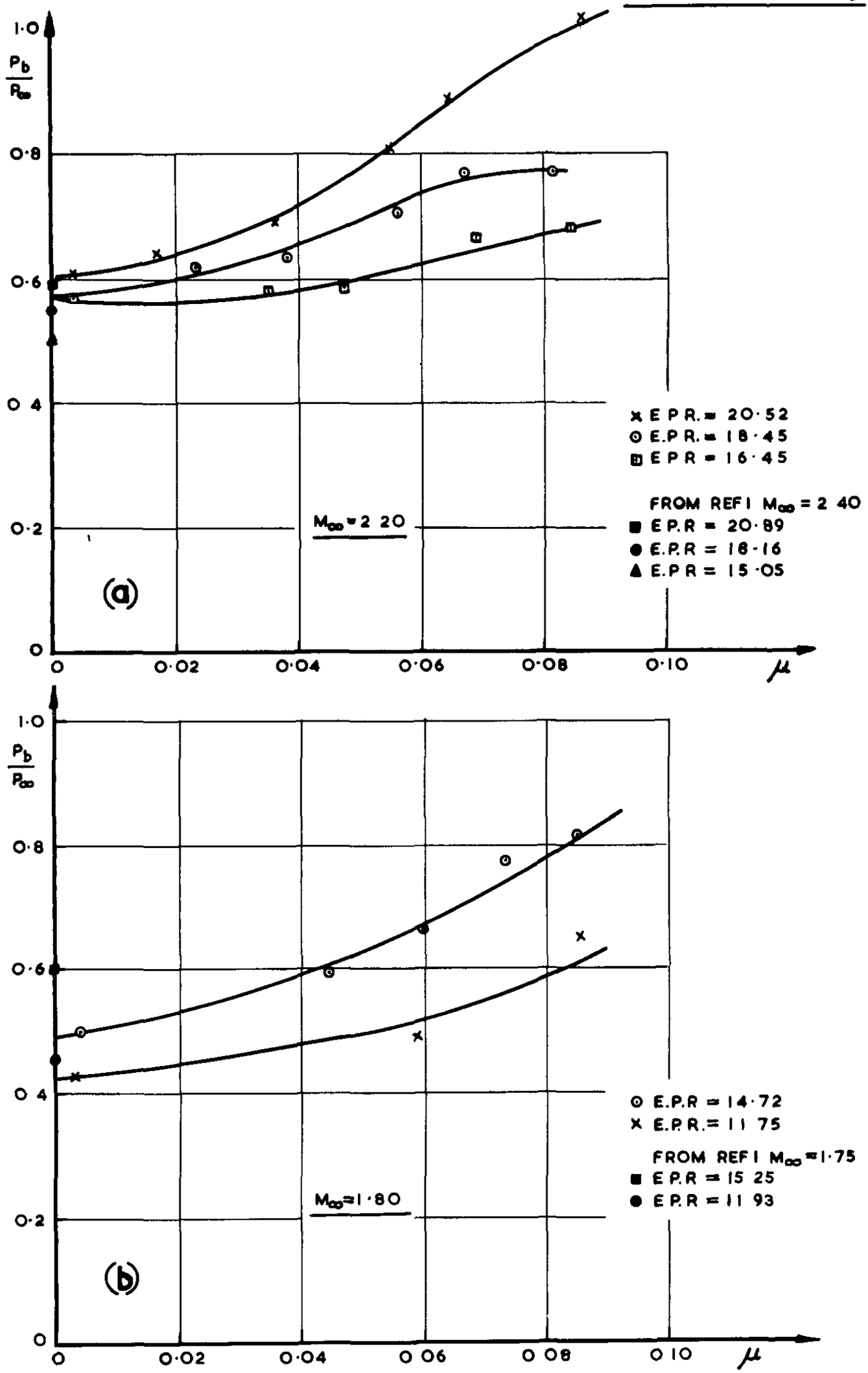

PERFORMANCE OF LONG NOZZLE WITH COPLANAR EXIT.

FIG. 15 (a & b)

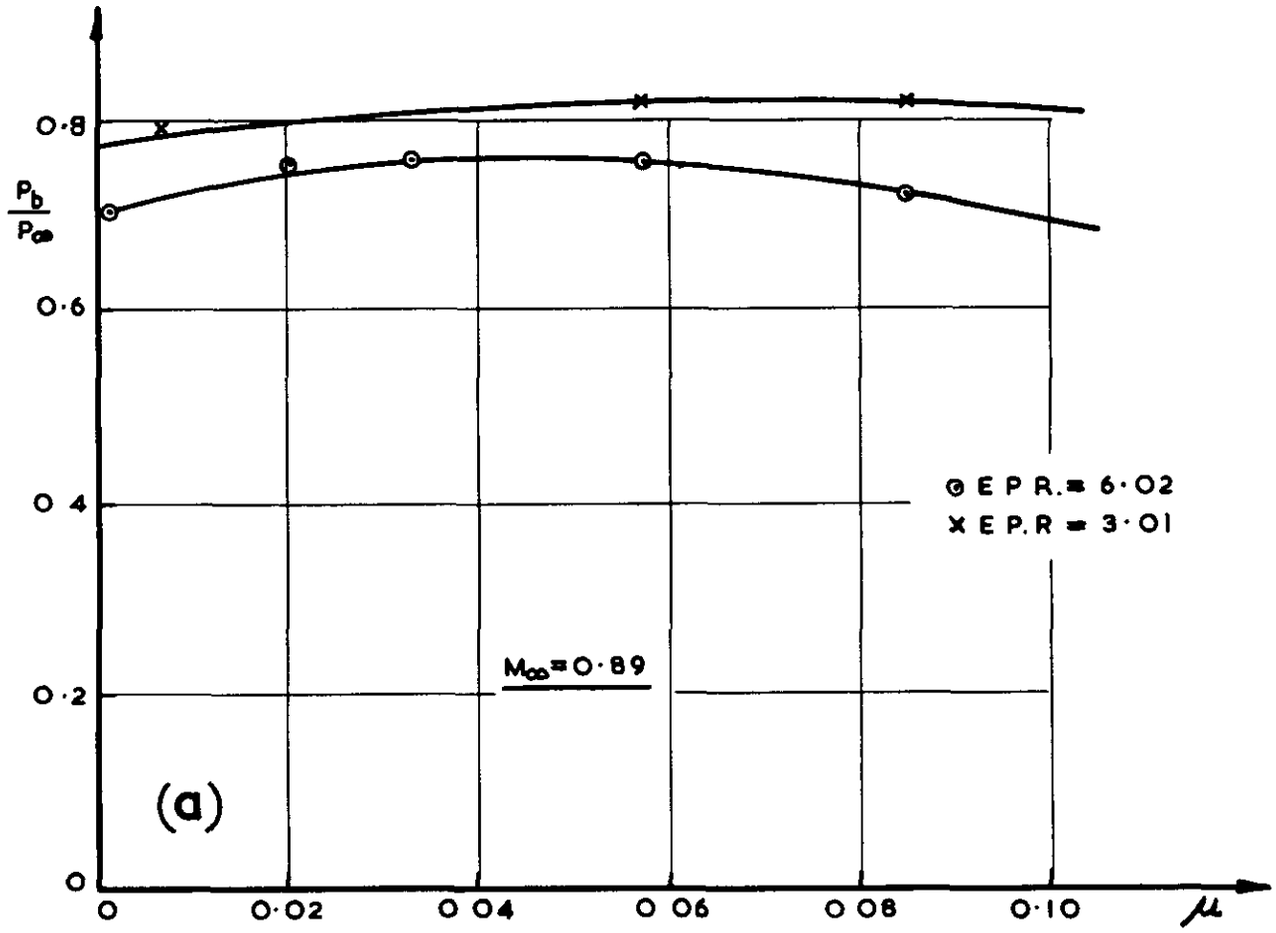

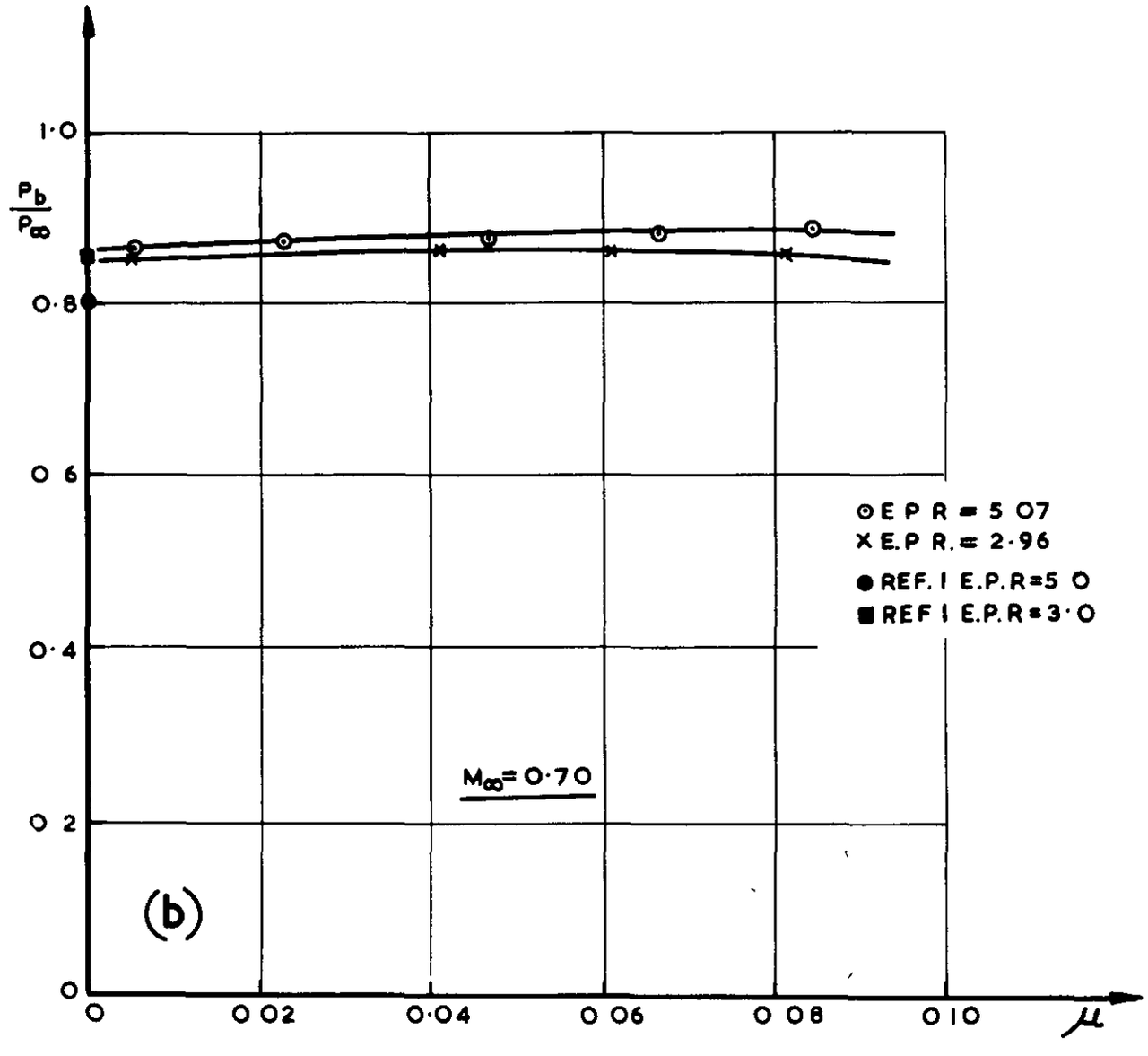

PERFORMANCE OF LONG NOZZLE WITH COPLANAR EXIT.

FIG.16

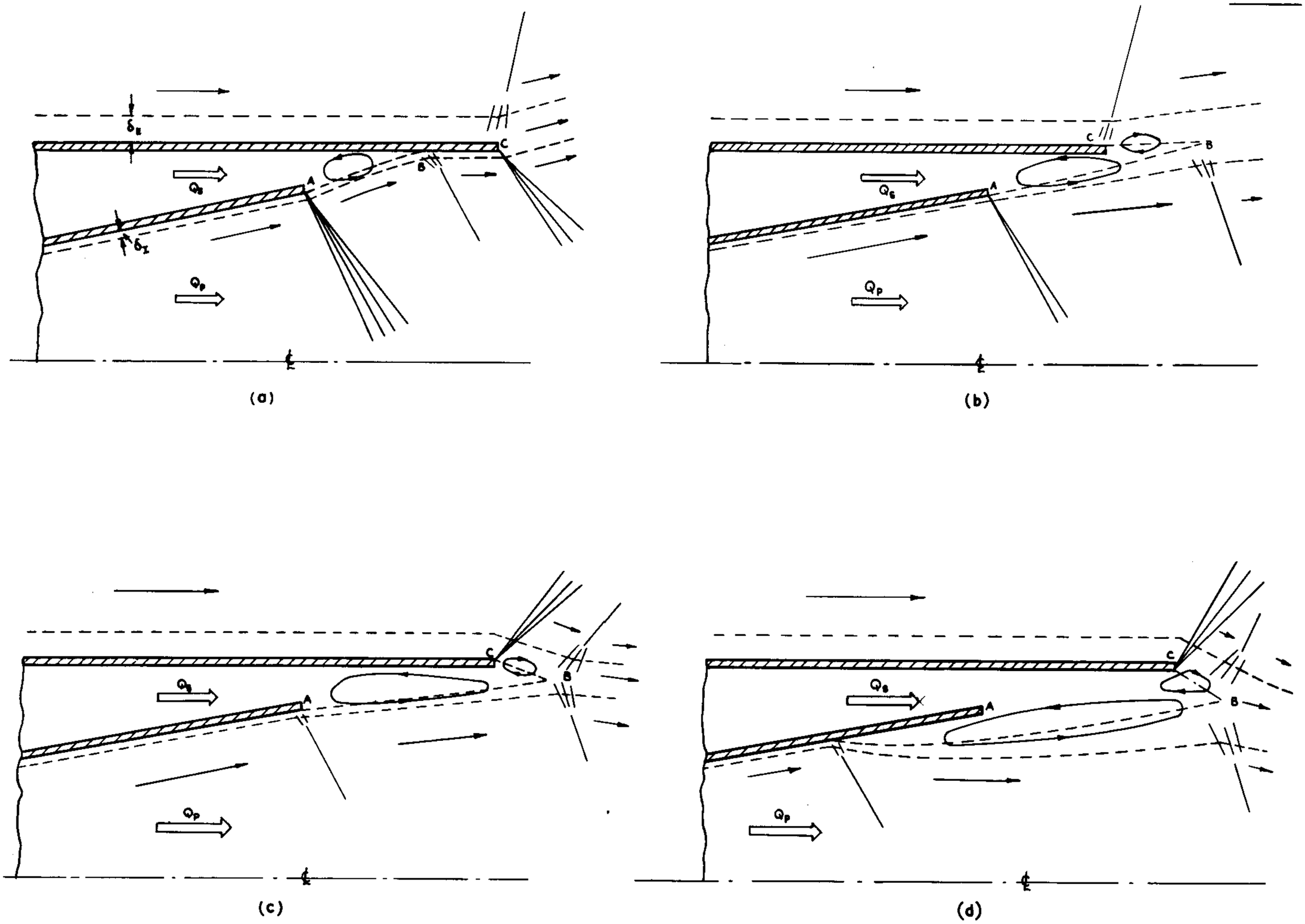

BASE FLOW PATTERNS FOR A NOZZLE WITH AN EXTENDED SHROUD, OPERATING IN EXTERNAL FLOW.

FIG. 17

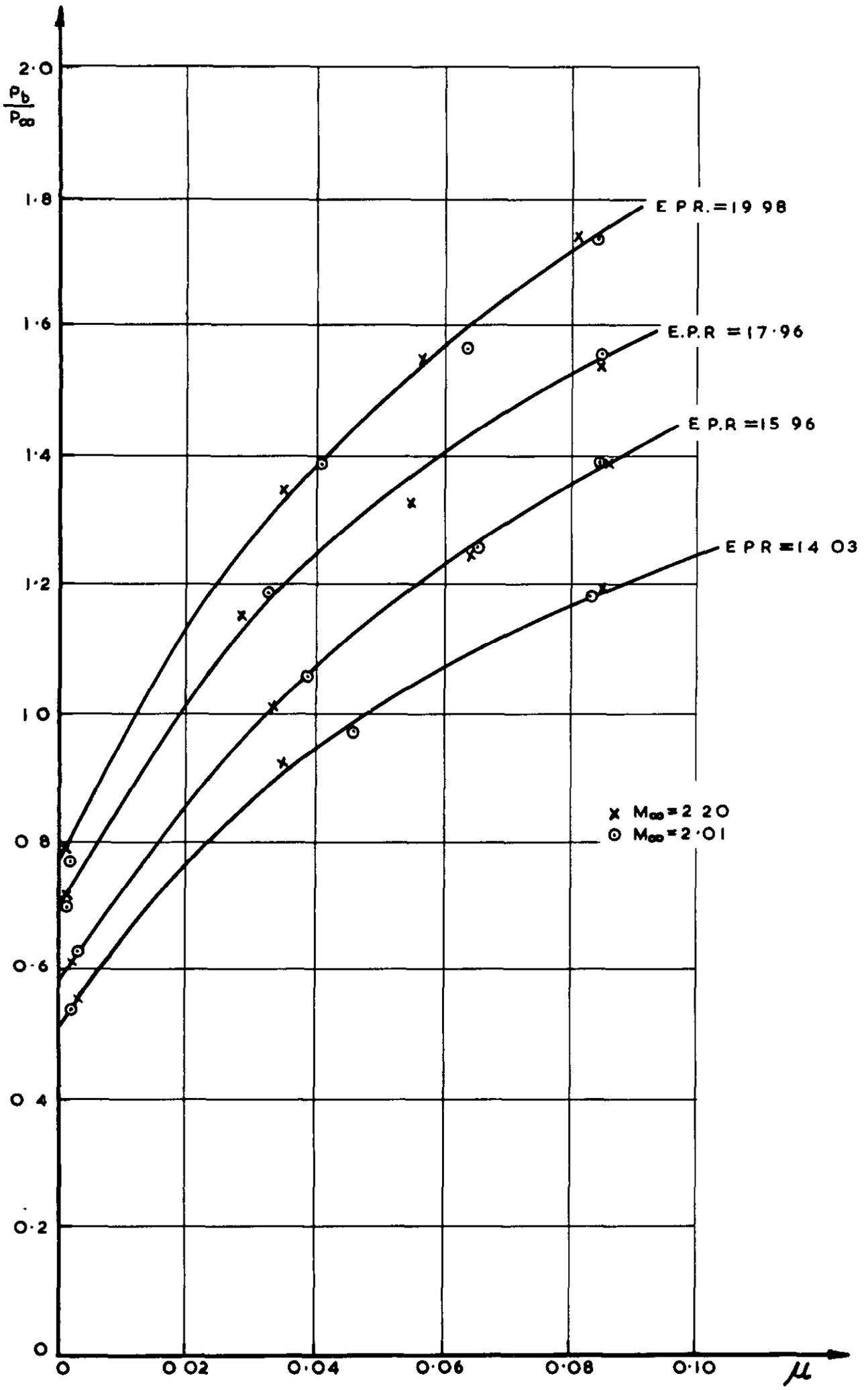

PERFORMANCE OF SHORT NOZZLE WITH EXTENDED SHROUD.

FIG. 18

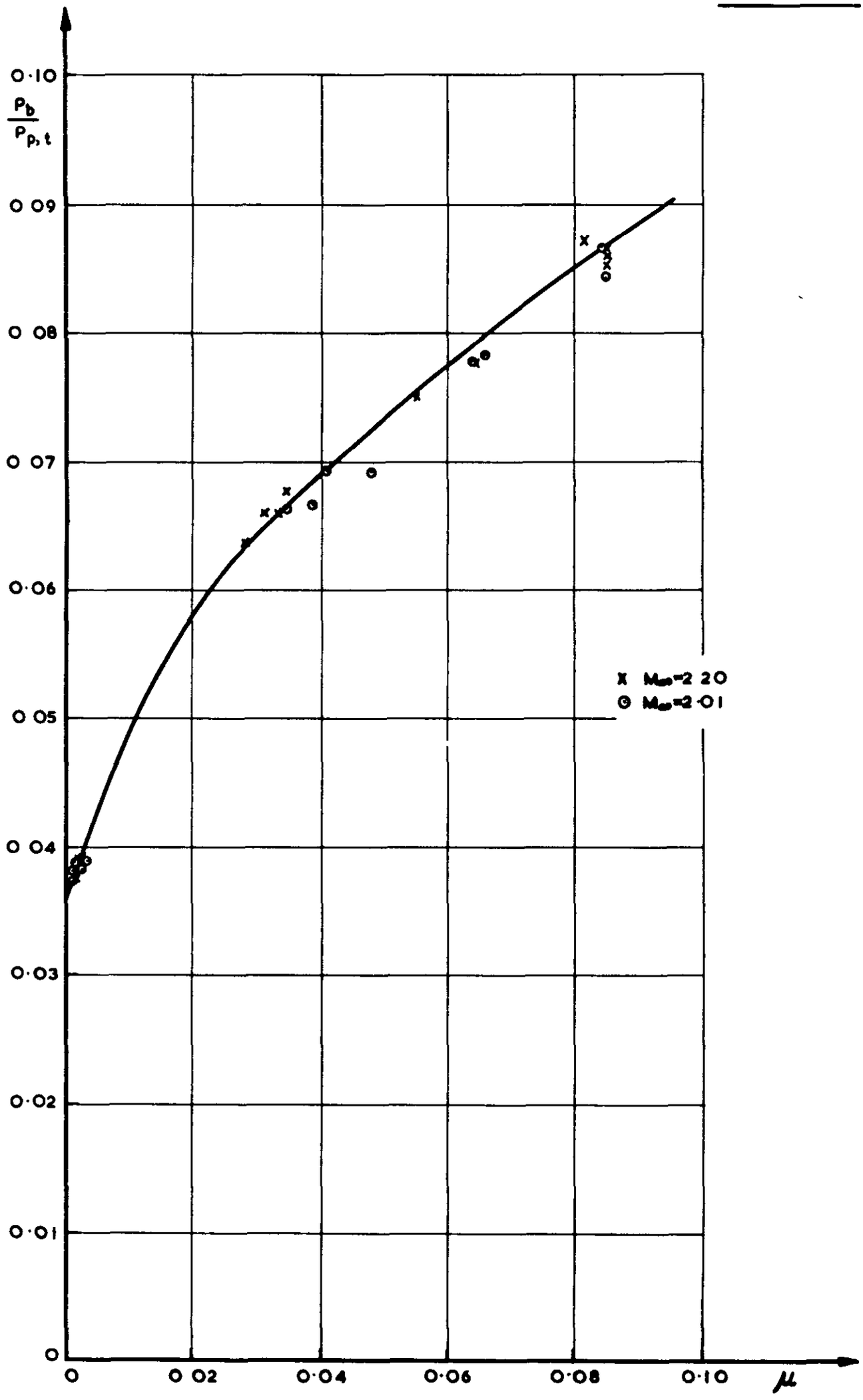

PERFORMANCE OF SHORT NOZZLE WITH EXTENDED SHROUD.

FIG. 19

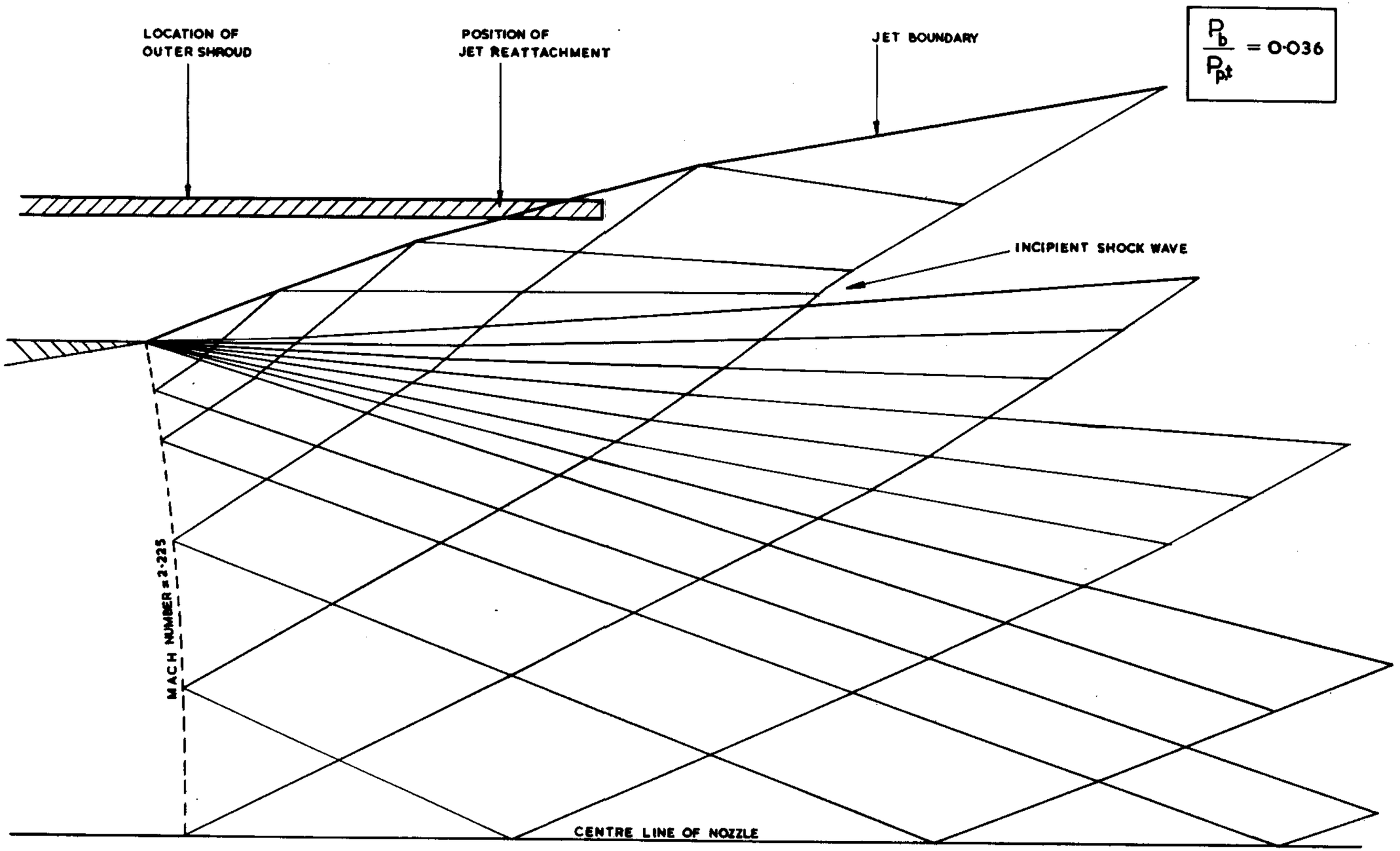

CONSTRUCTION OF THE ISOBARIC JET BOUNDARY BY AXIALLY SYMMETRIC CHARACTERISTICS.
(WITH SUPERIMPOSED OUTER SHROUD LOCATION.)

FIG.20

$\frac{P_b}{P_{pt}} = 0085$

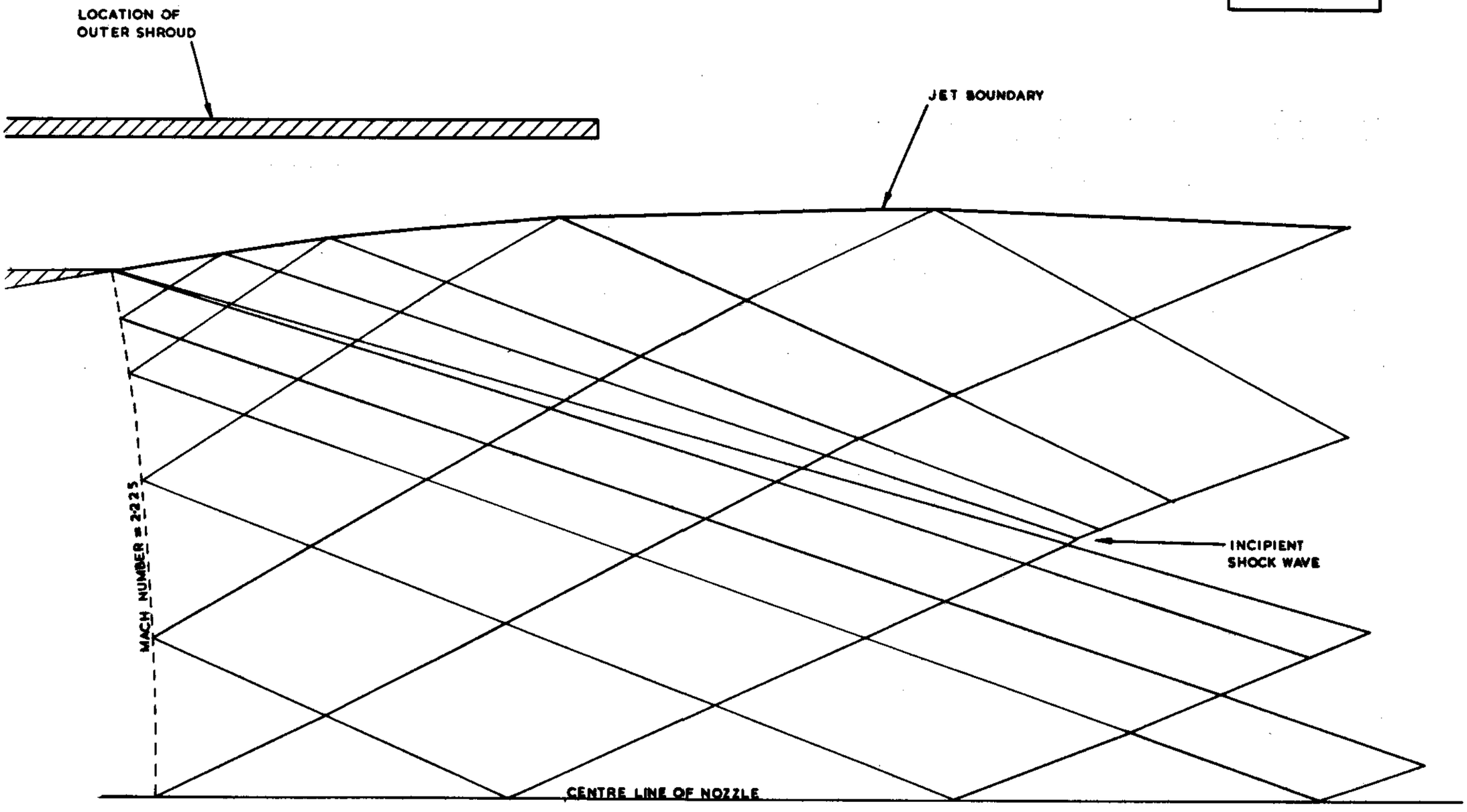

CONSTRUCTION OF THE ISOBARIC JET BOUNDARY BY AXIALLY SYMMETRIC CHARACTERISTICS.
(WITH SUPERIMPOSED OUTER SHROUD LOCATION.)

FIG. 21.(a&b)

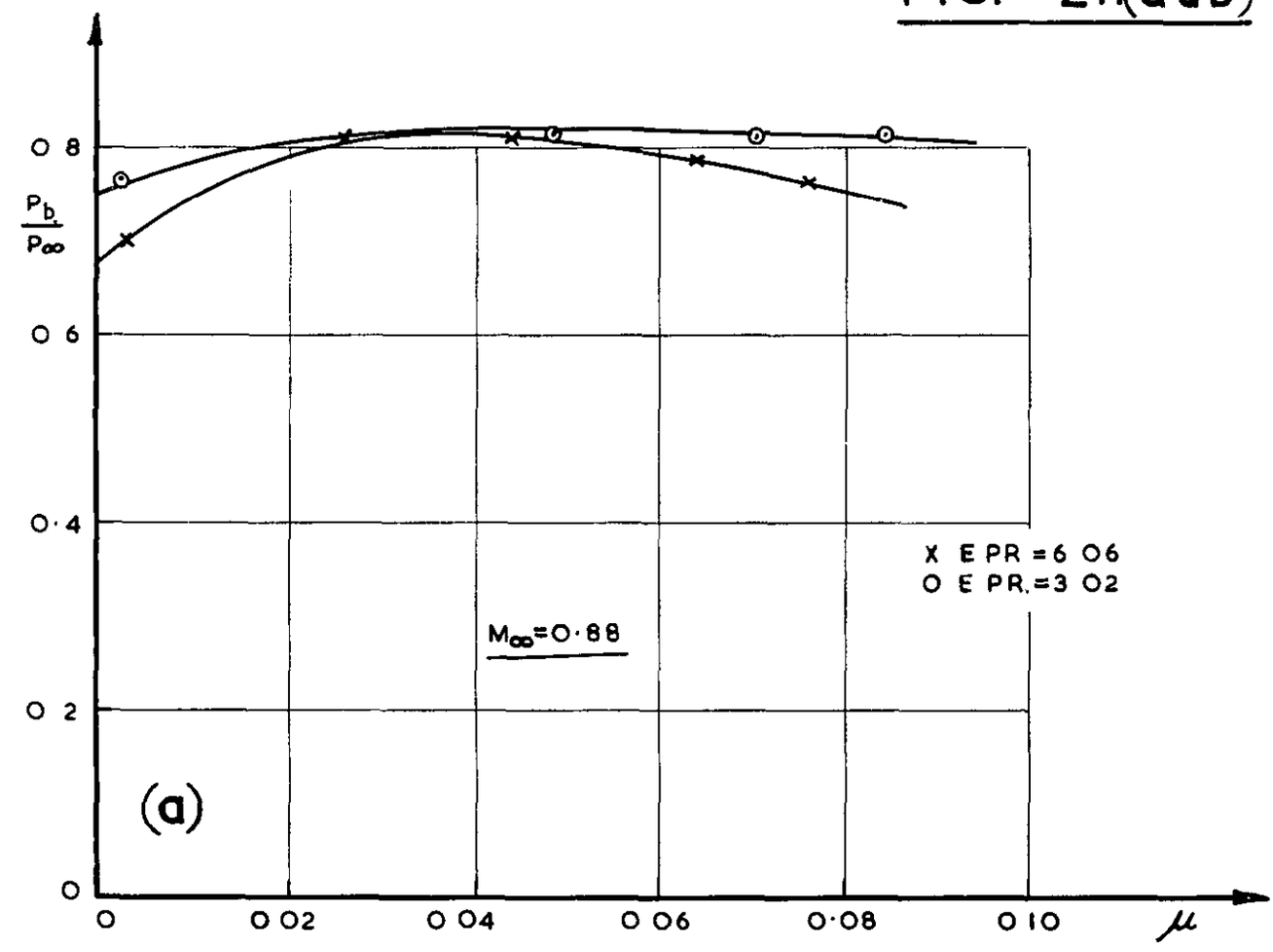

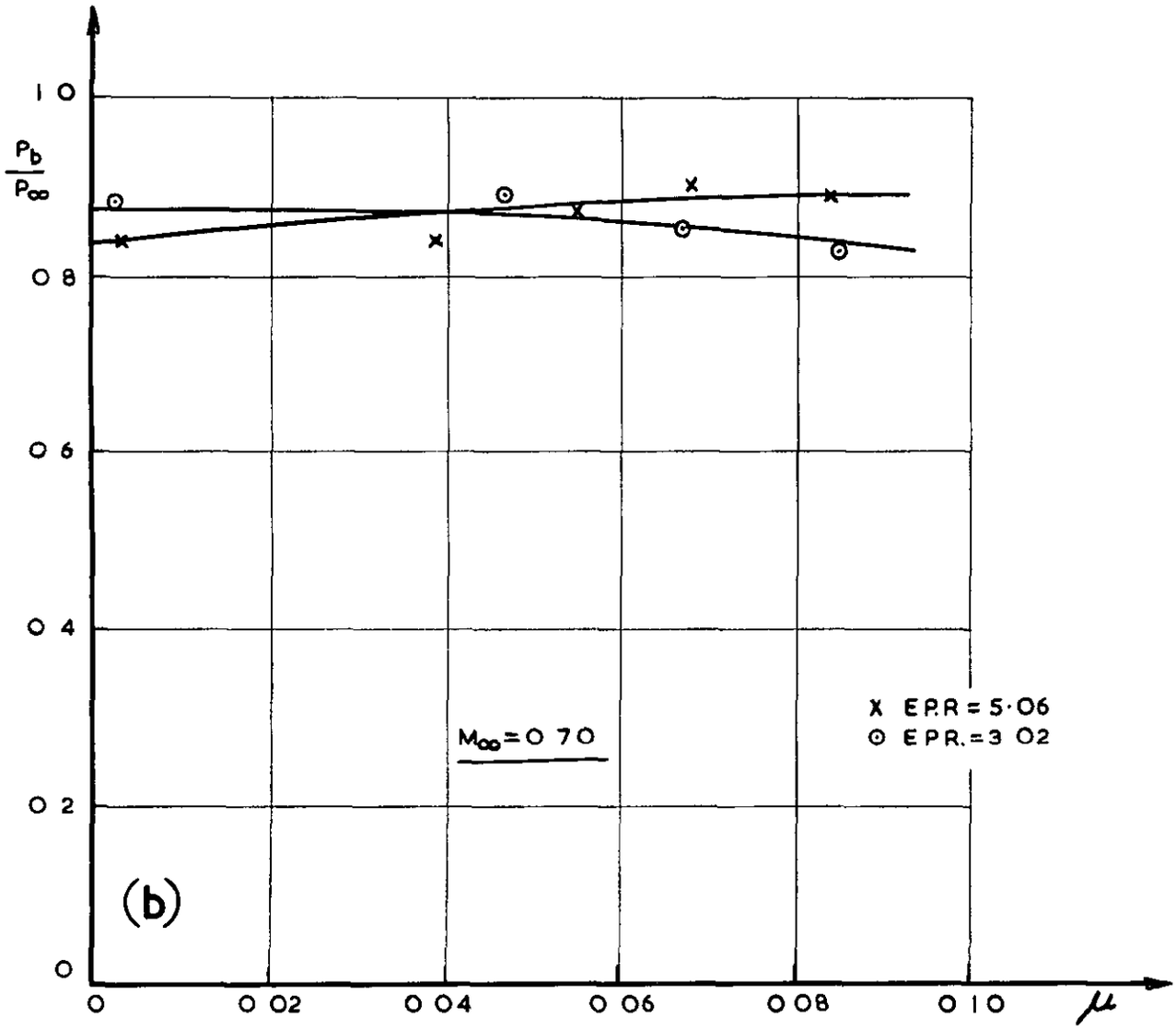

PERFORMANCE OF SHORT NOZZLE WITH EXTENDED SHROUD.

FIG. 22 (a & b)

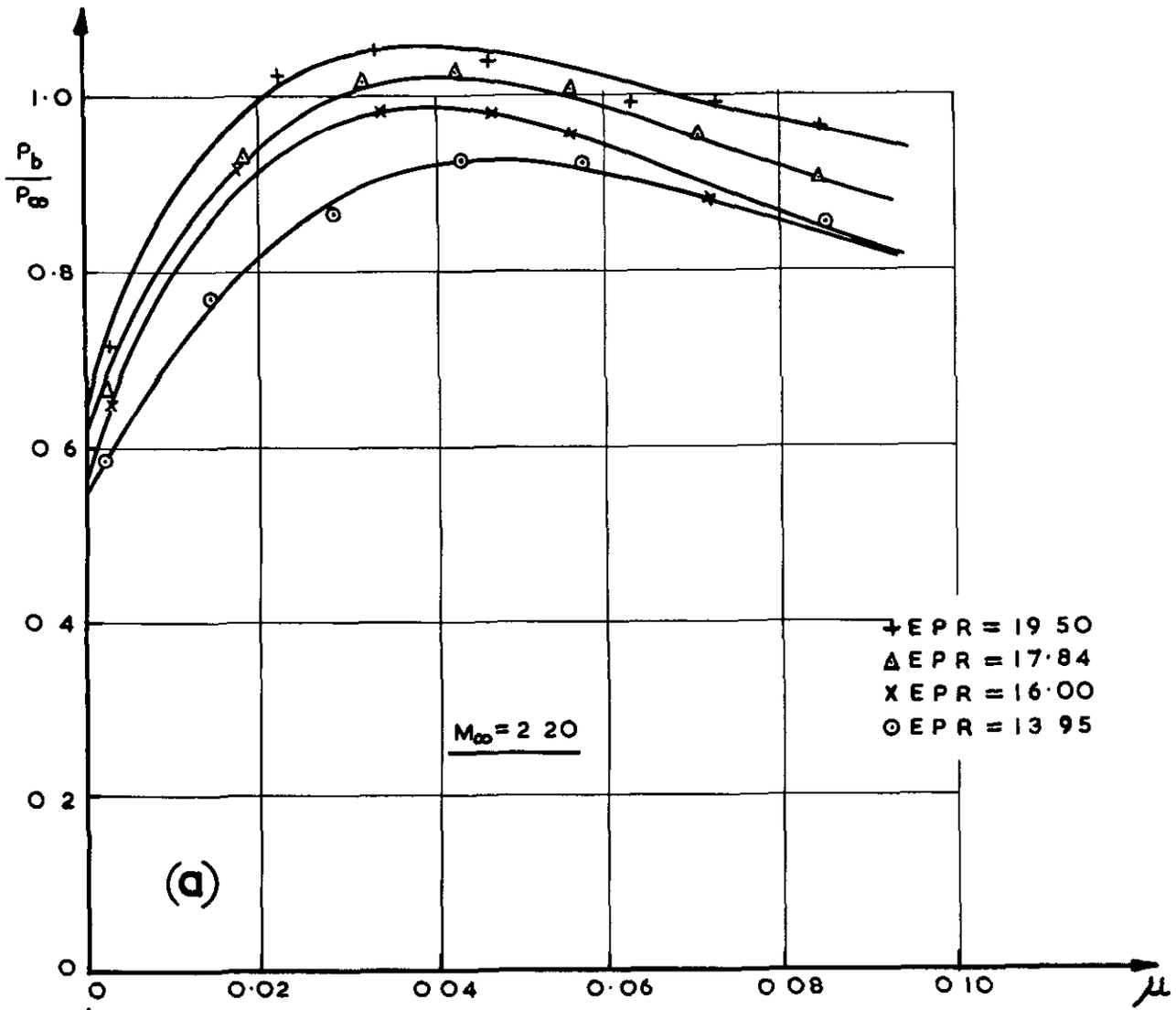

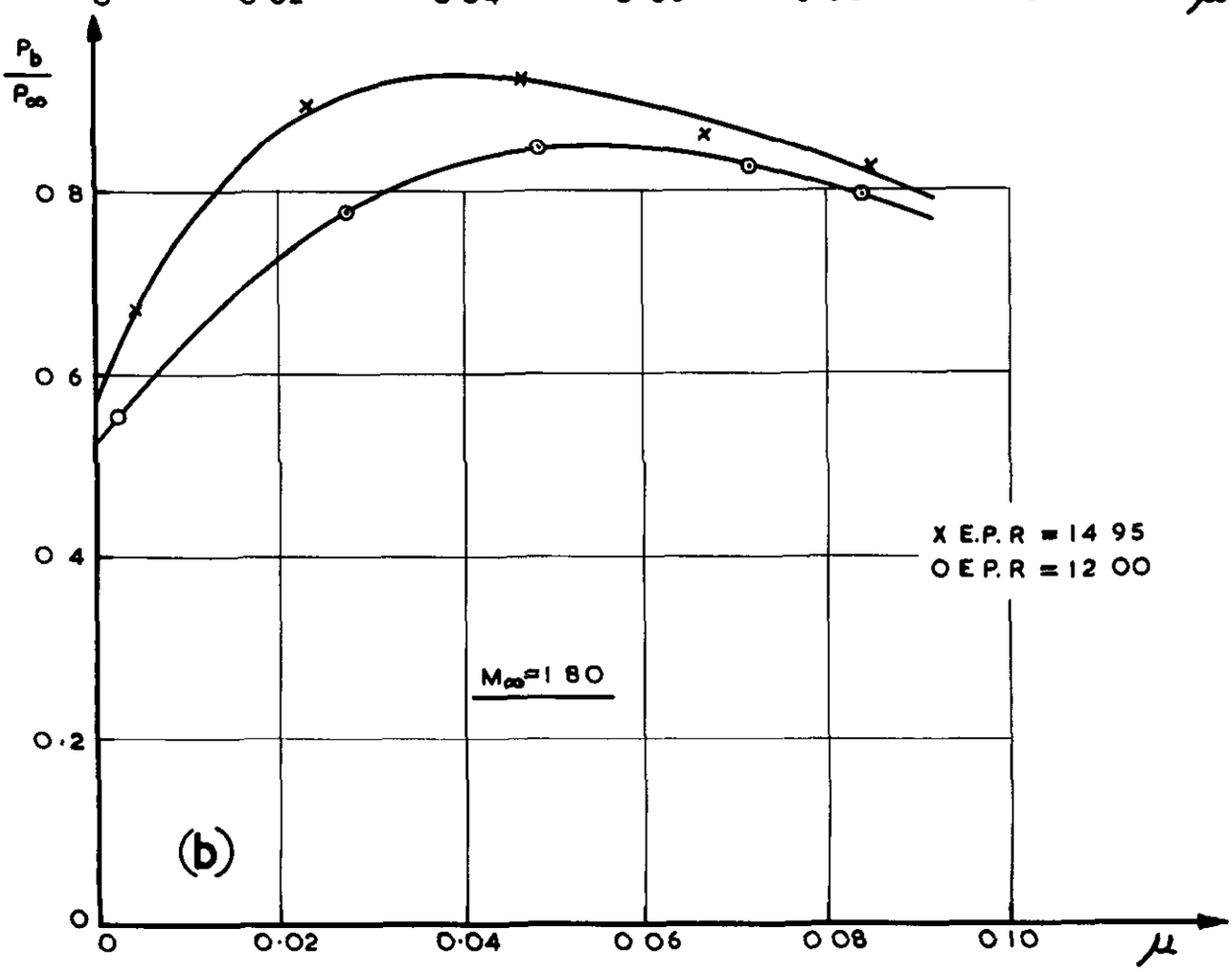

PERFORMANCE OF SHORT NOZZLE WITH BOAT-TAILED EXTERIOR.

FIG. 23 (a&b)

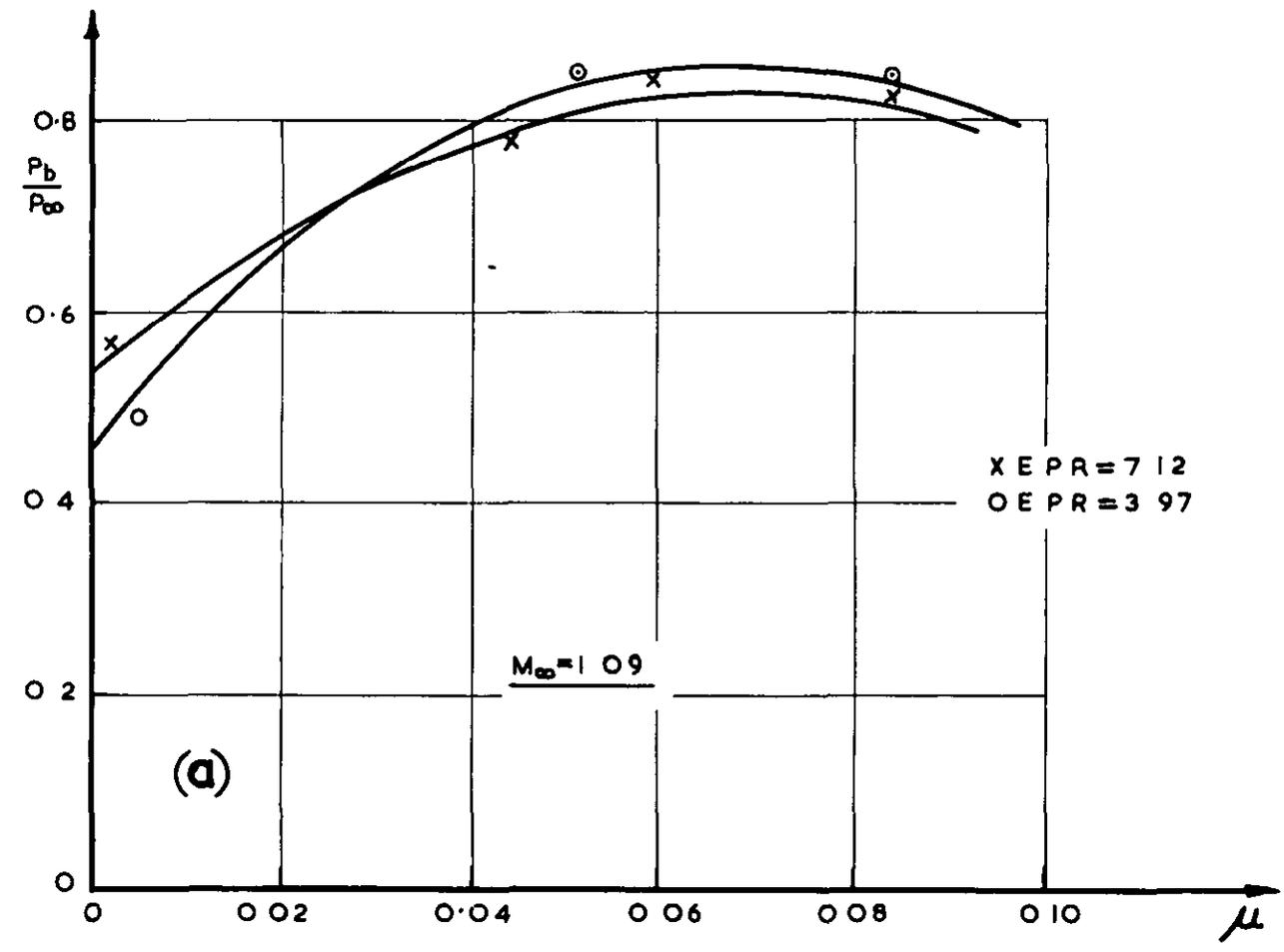

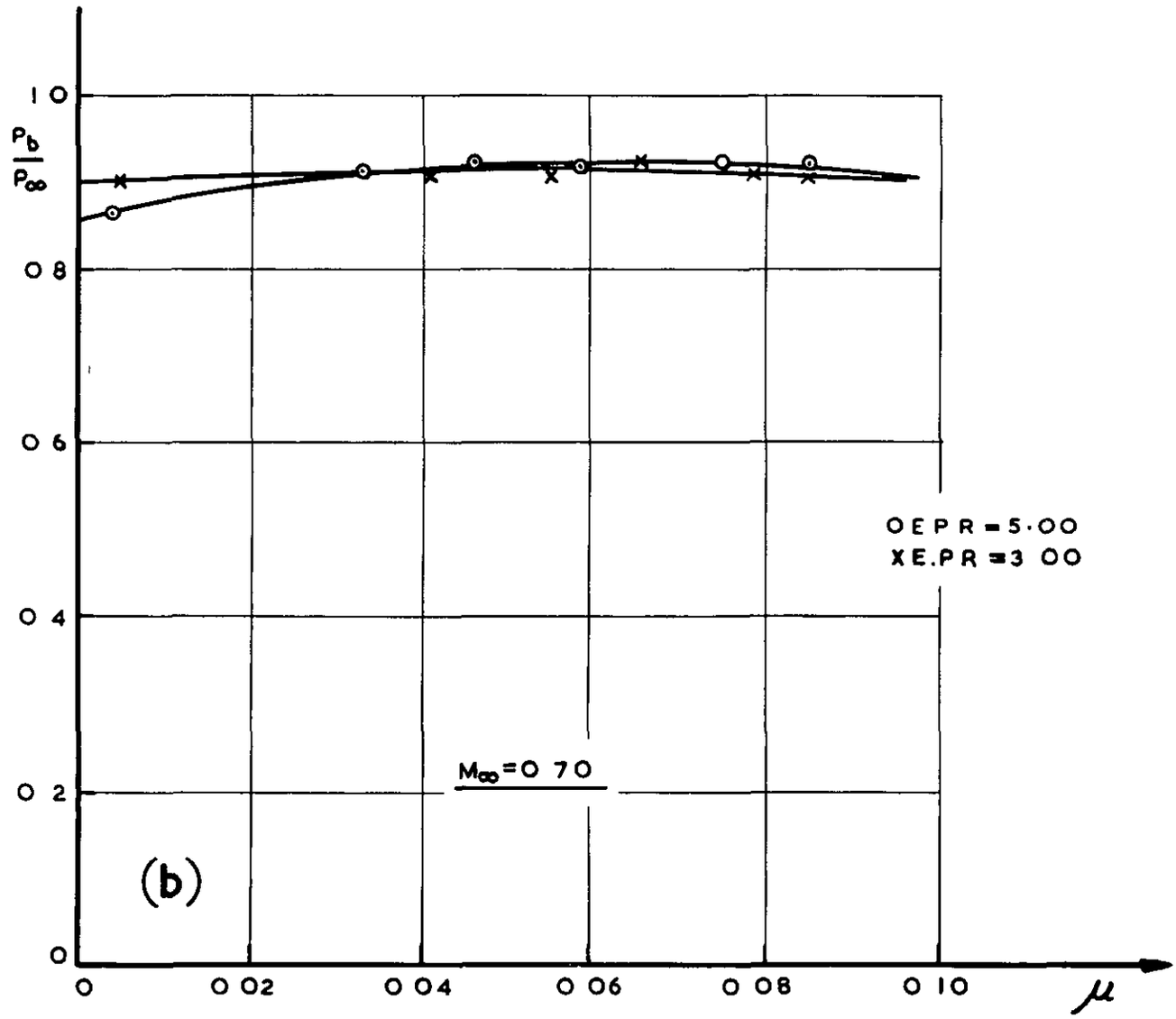

PERFORMANCE OF SHORT NOZZLE WITH BOAT-TAILED EXTERIOR.

FIG. 24 (a & b)

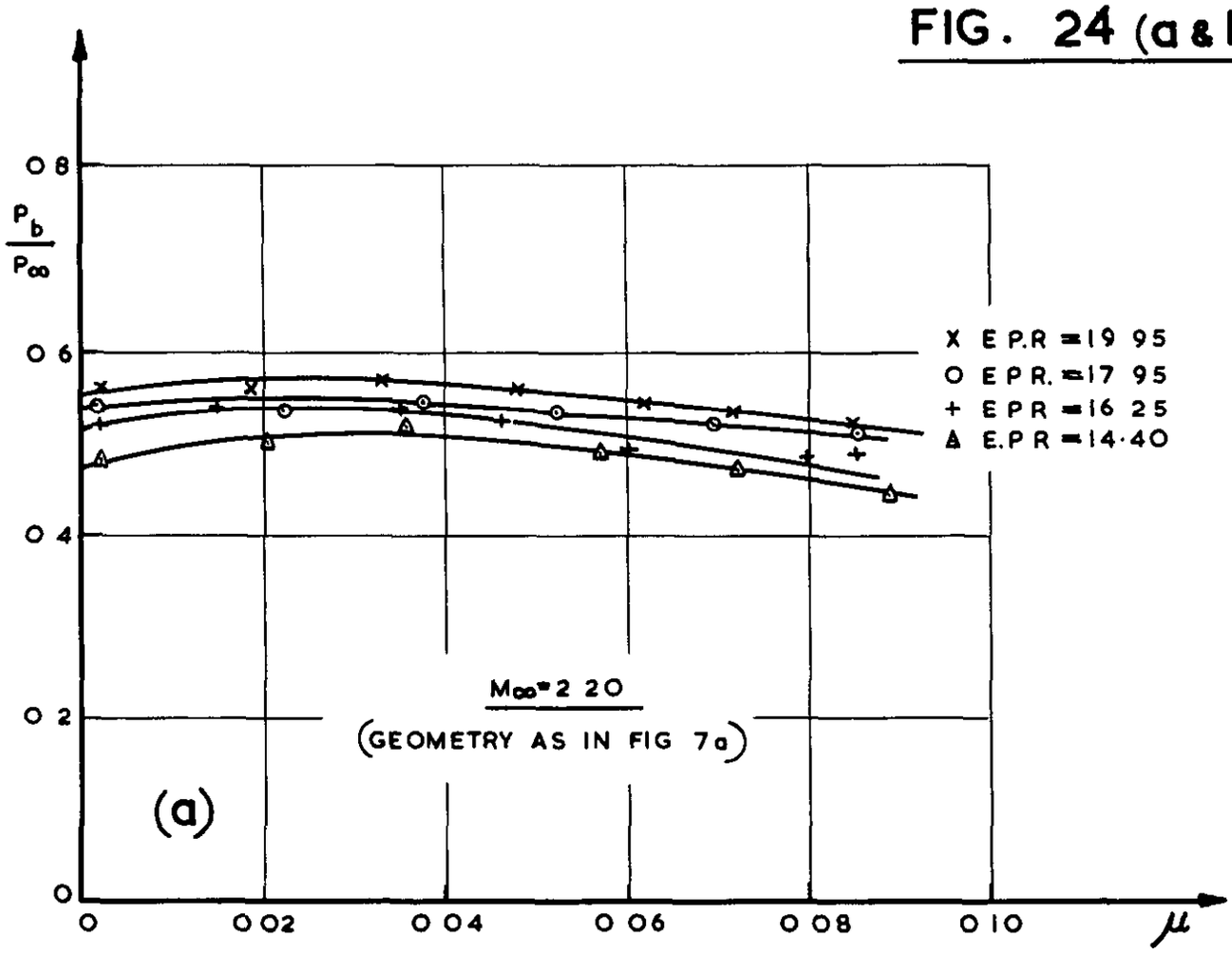

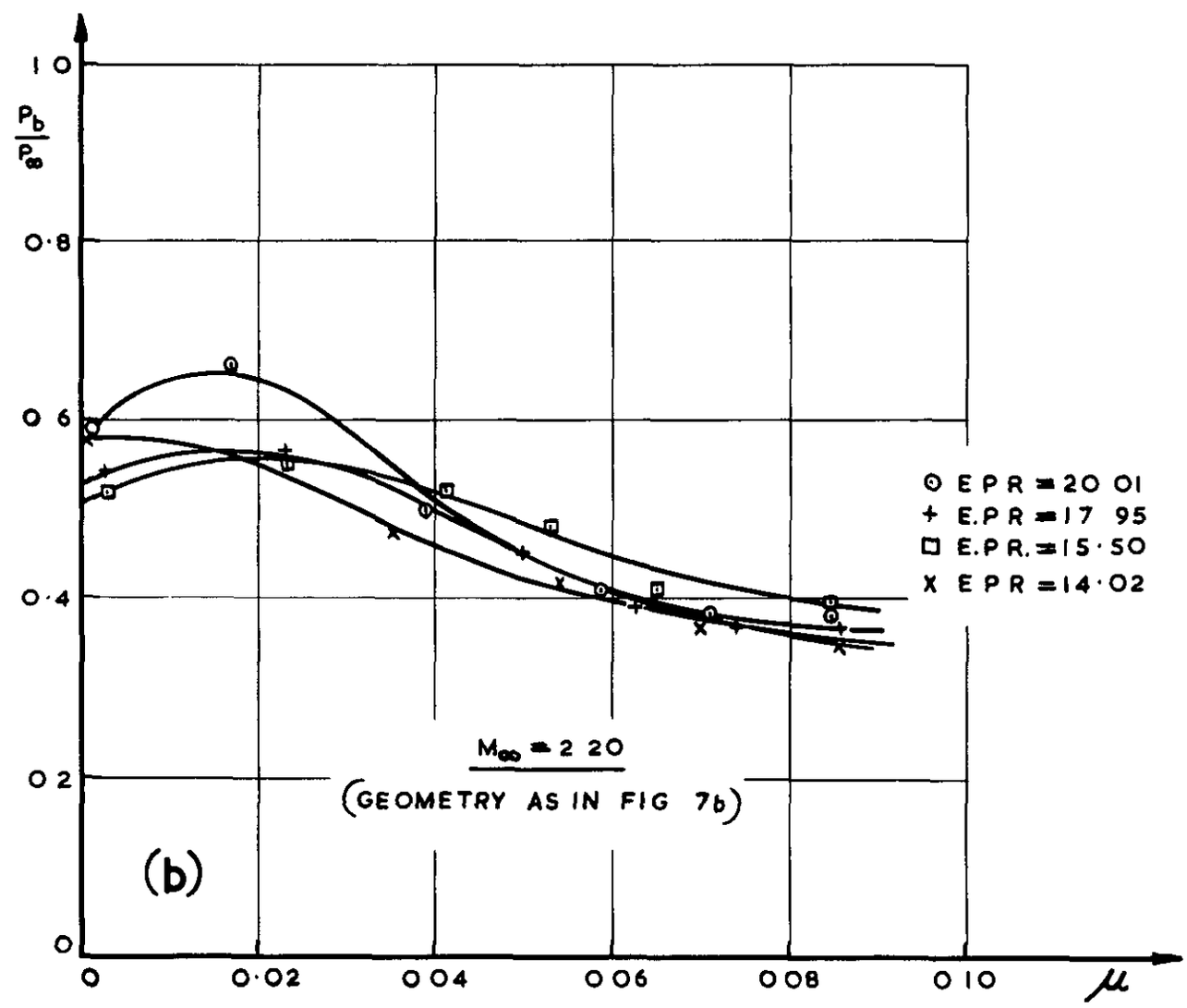

PERFORMANCE OF SHORT NOZZLE WITH BASE BLOCKAGE.

FIG. 25

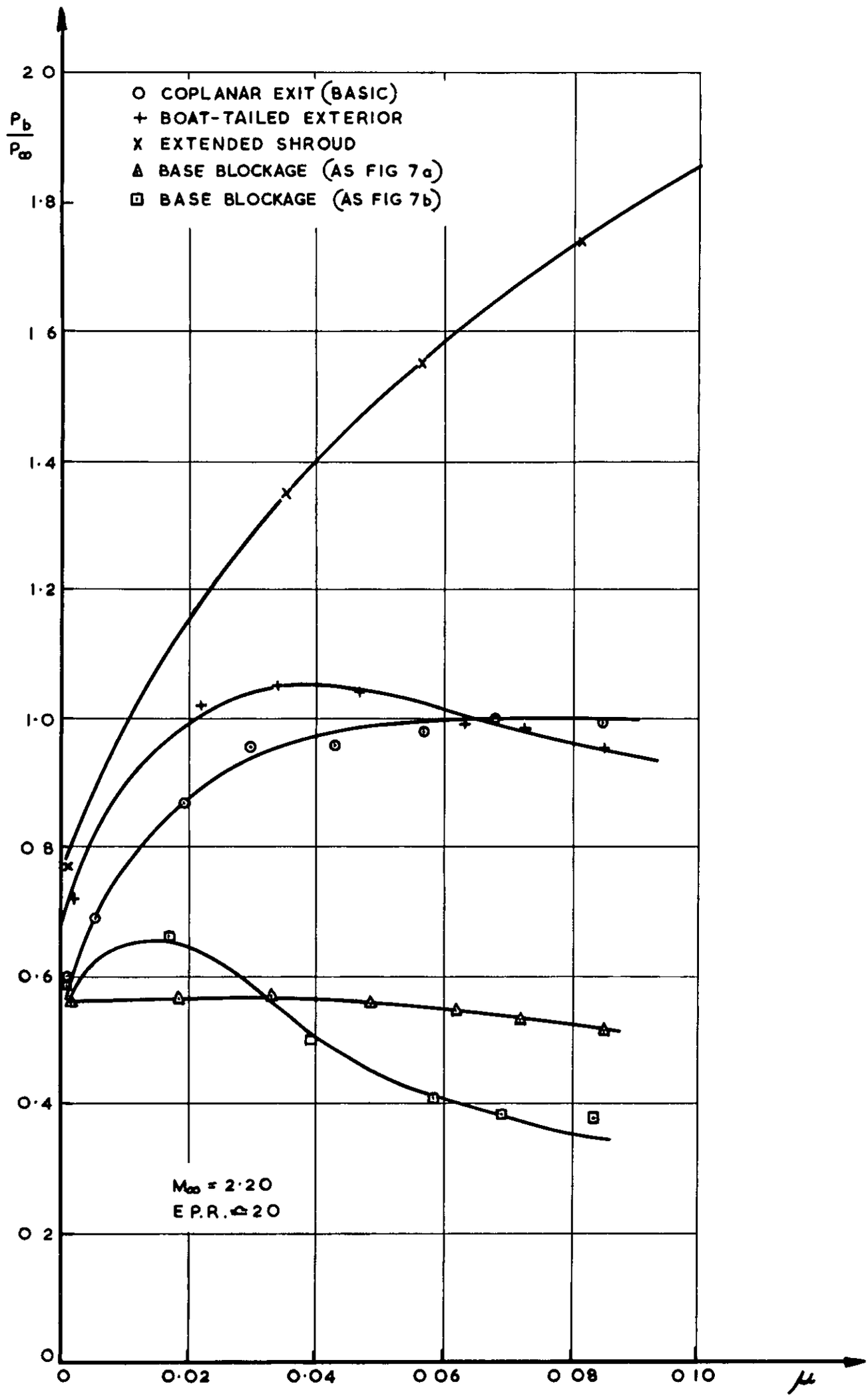

COMPARISON OF RESULTS FROM SHORT NOZZLES.

FIG. 26

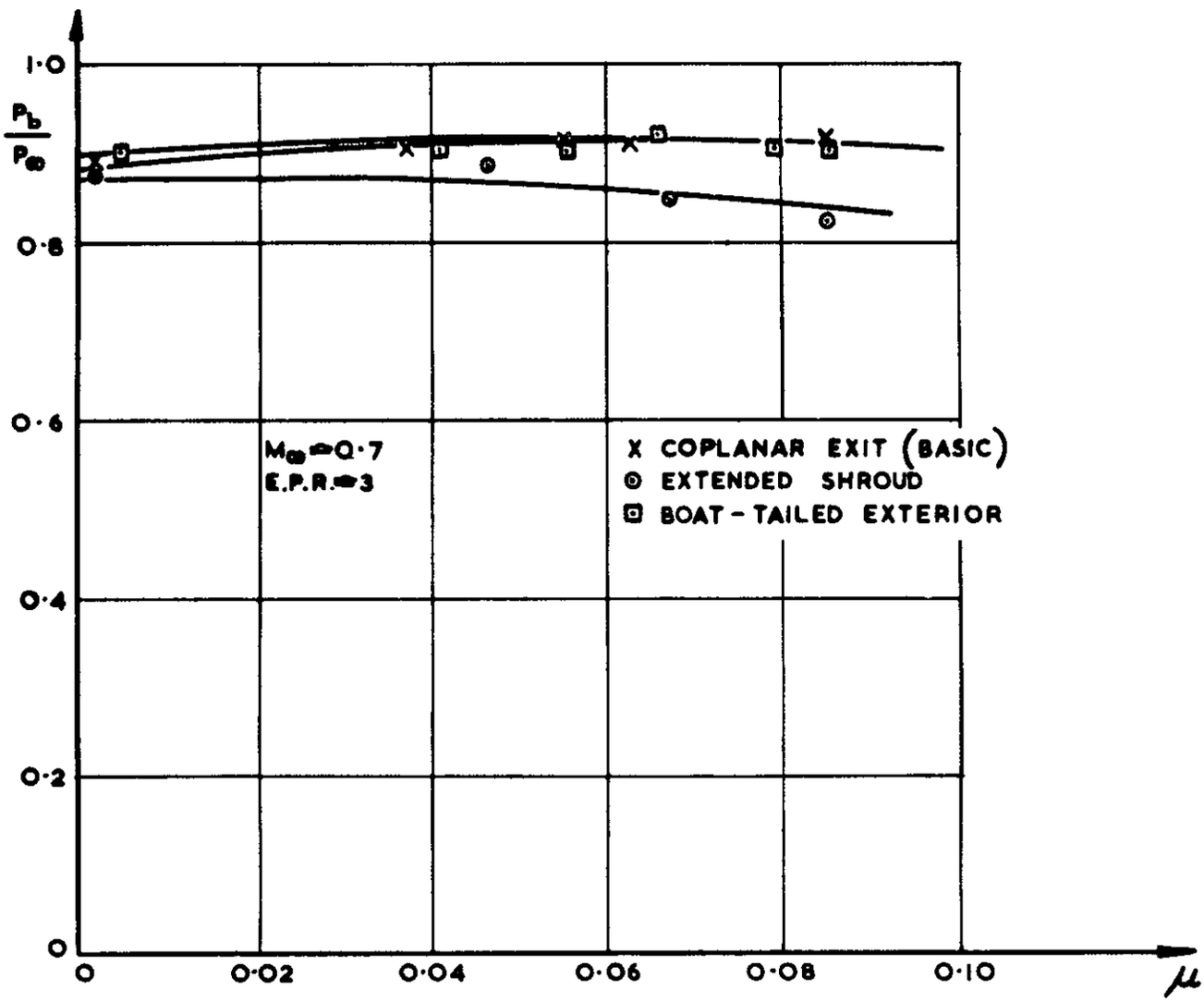

COMPARISON OF RESULTS FROM SHORT NOZZLES.

FIG. 27

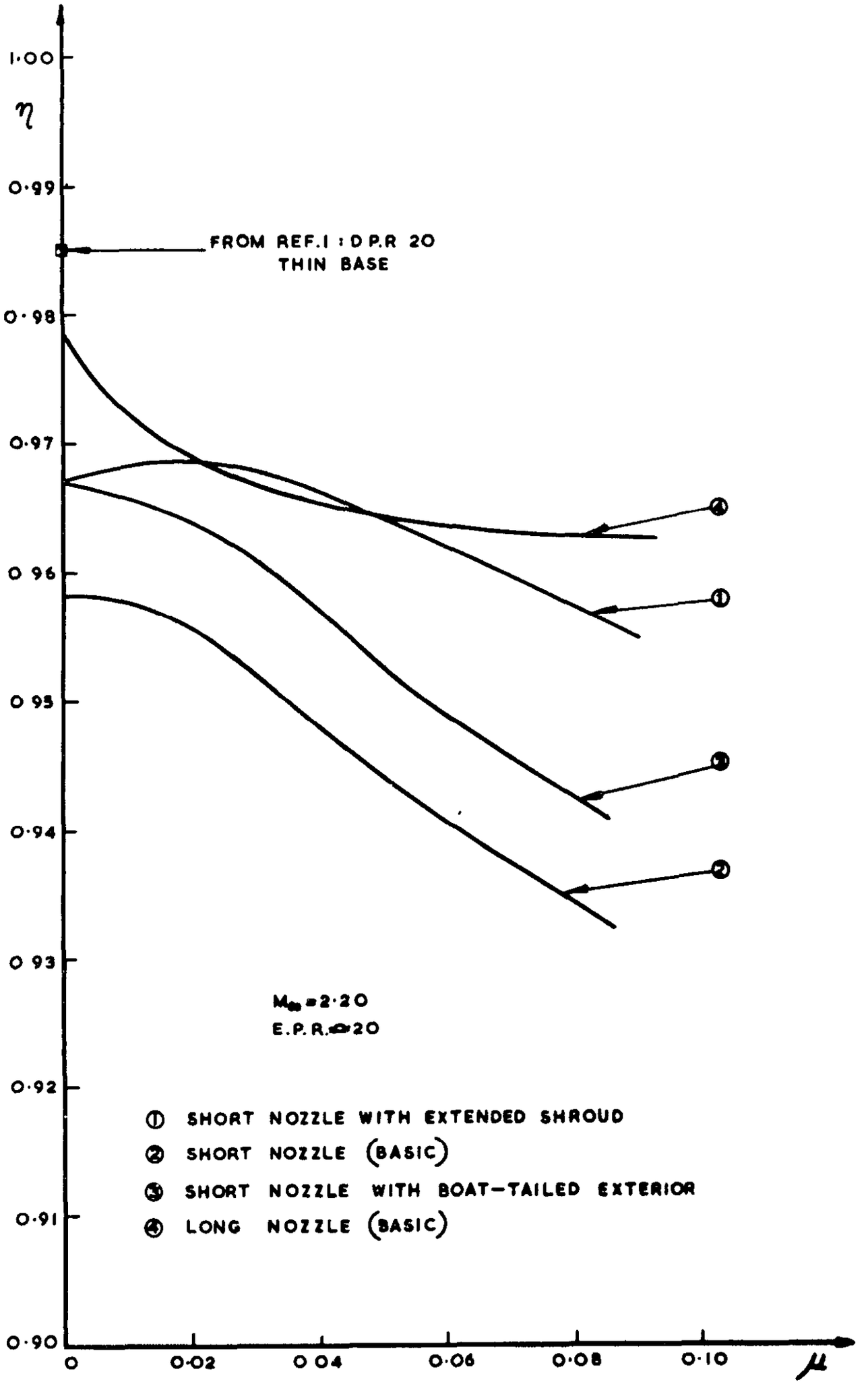

COMPARISON OF OVERALL EFFICIENCIES.

FIG. 28

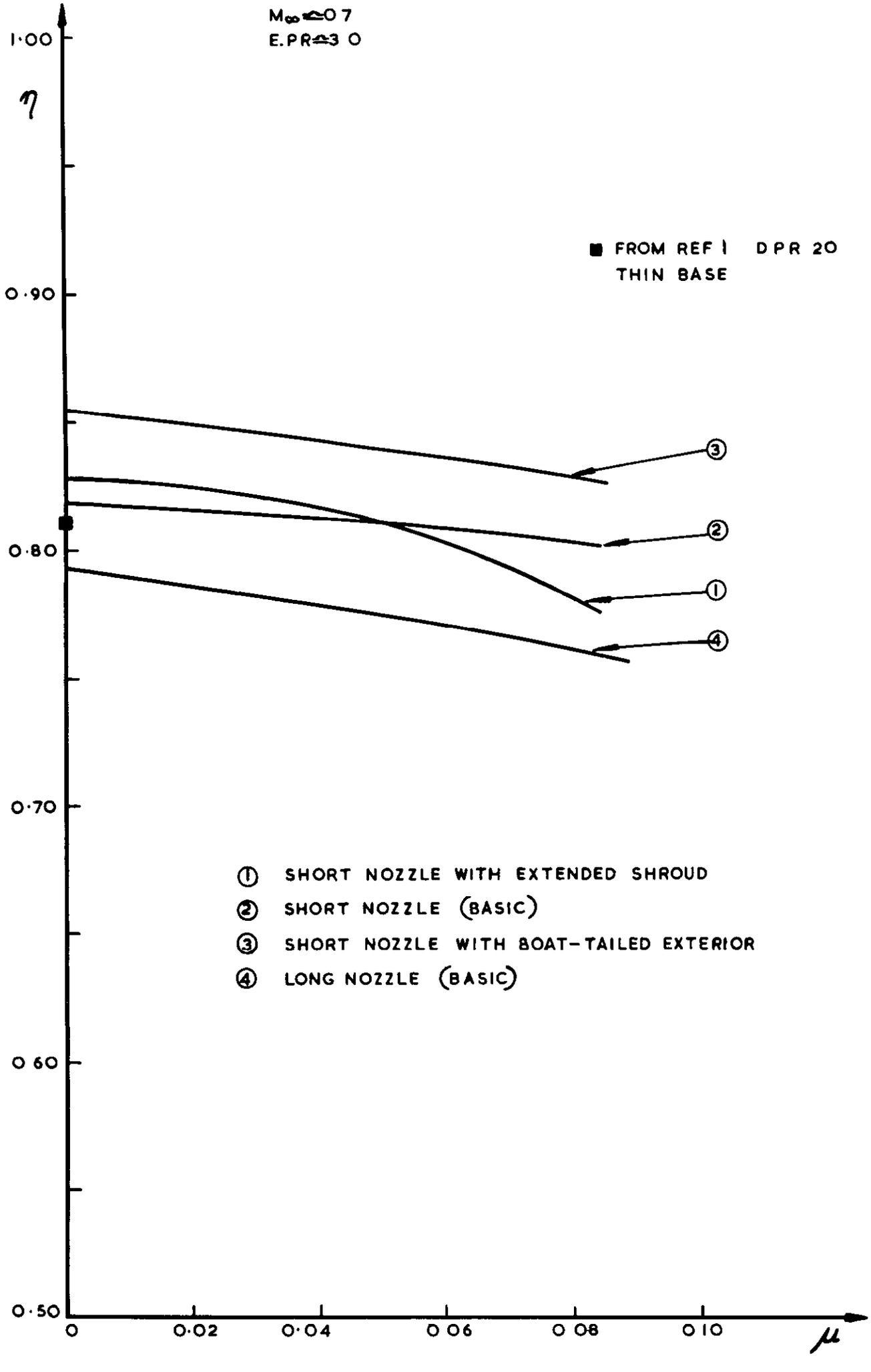

COMPARISON OF OVERALL EFFICIENCIES.

FIG. 29

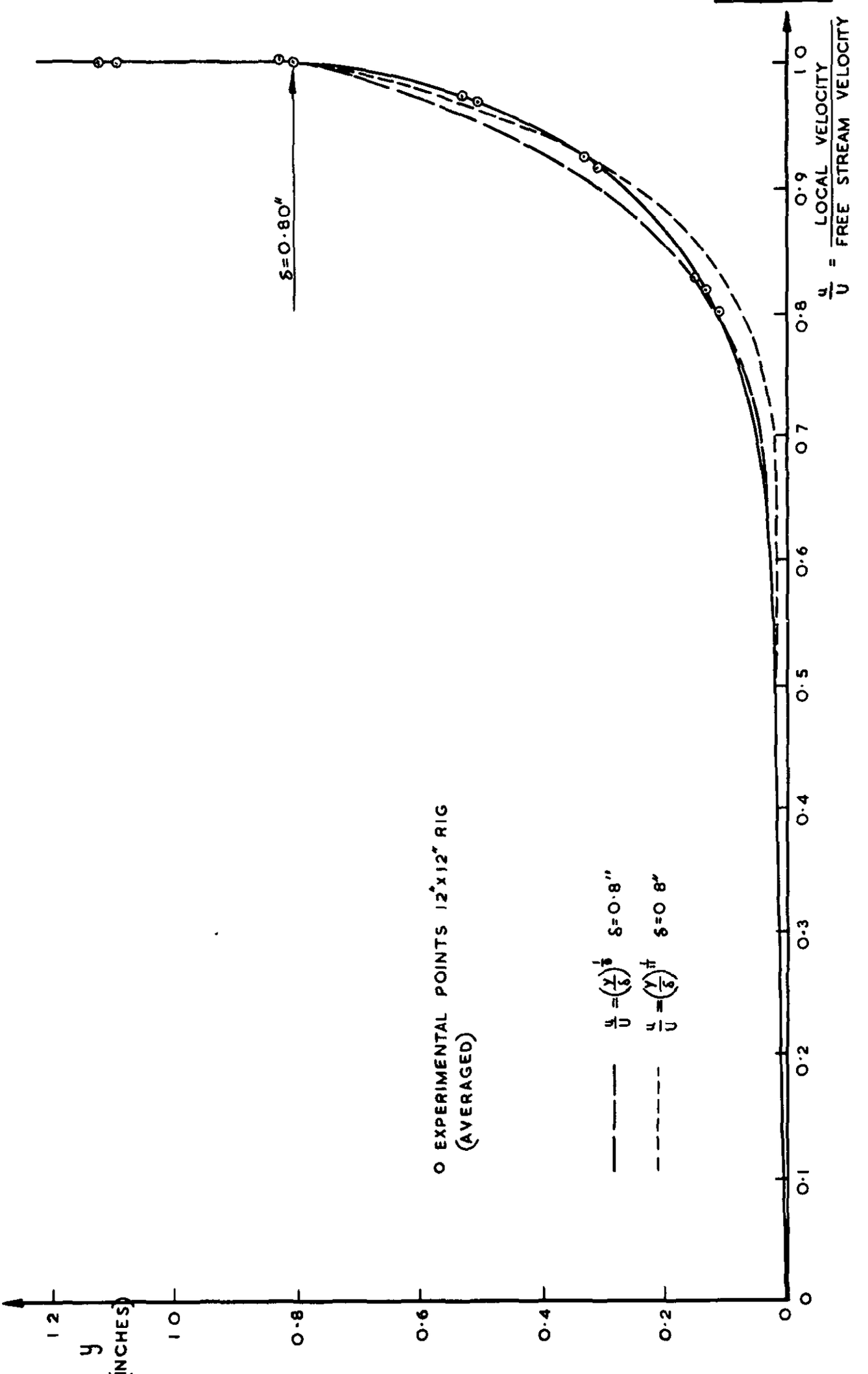

EXTERNAL BOUNDARY LAYER VELOCITY PROFILE.

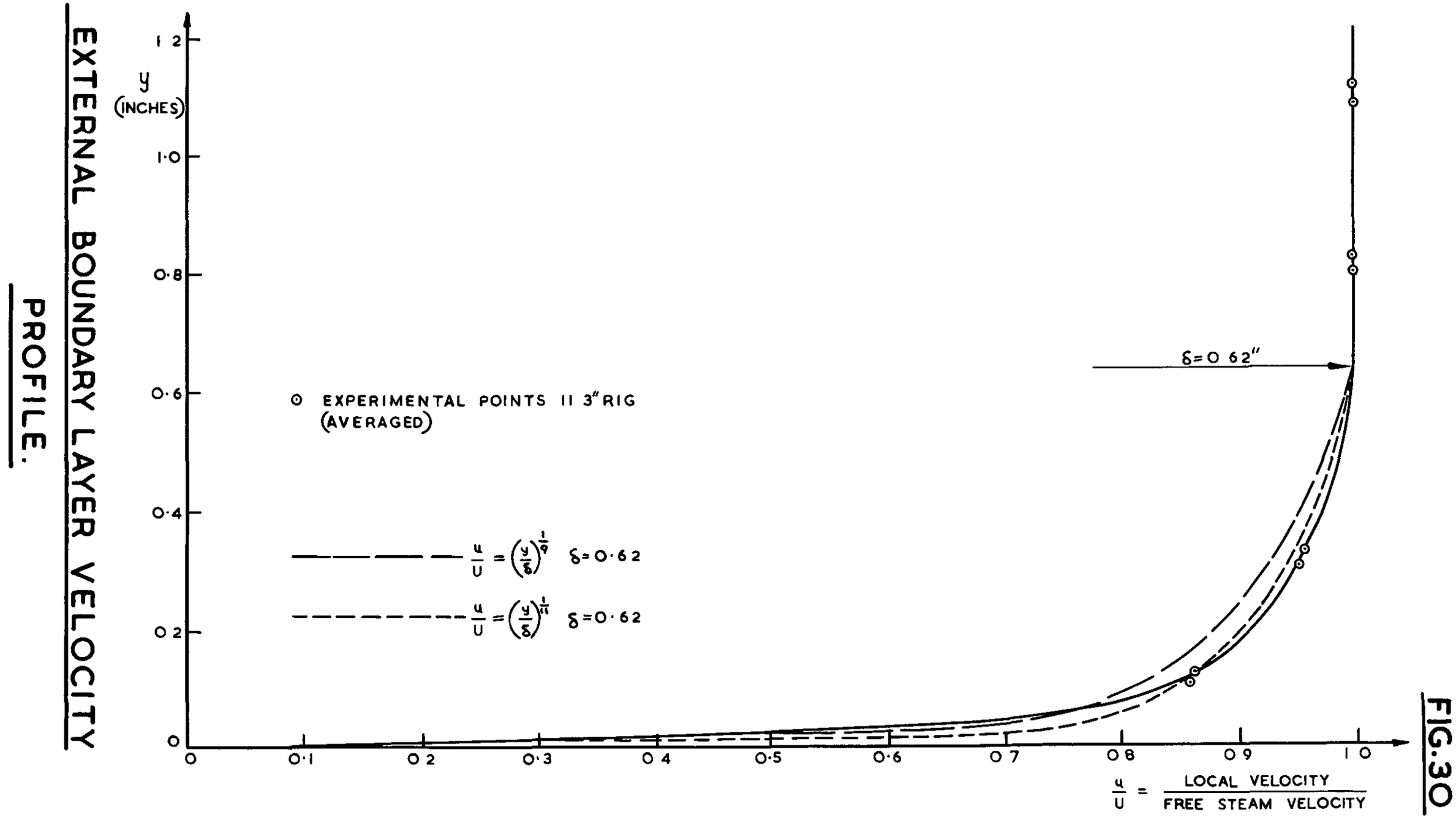
EXTERNAL BOUNDARY LAYER VELOCITY PROFILE.
y (INCHES)
1·2
1·0
0·8
0·6
0·4
0·2
0
0·1
0·2
0·3
0·4
0·5
0·6
0·7
0·8
0·9
1·0
δ=0·62"
⊙ EXPERIMENTAL POINTS 11 3" RIG (AVERAGED)
$\frac{u}{U} = \left(\frac{y}{\delta}\right)^{\frac{1}{9}}$ δ=0·62
$\frac{u}{U} = \left(\frac{y}{\delta}\right)^{\frac{1}{11}}$ δ=0·62
$\frac{u}{U}$ = LOCAL VELOCITY / FREE STEAM VELOCITY

FIG.30

FIG. 31

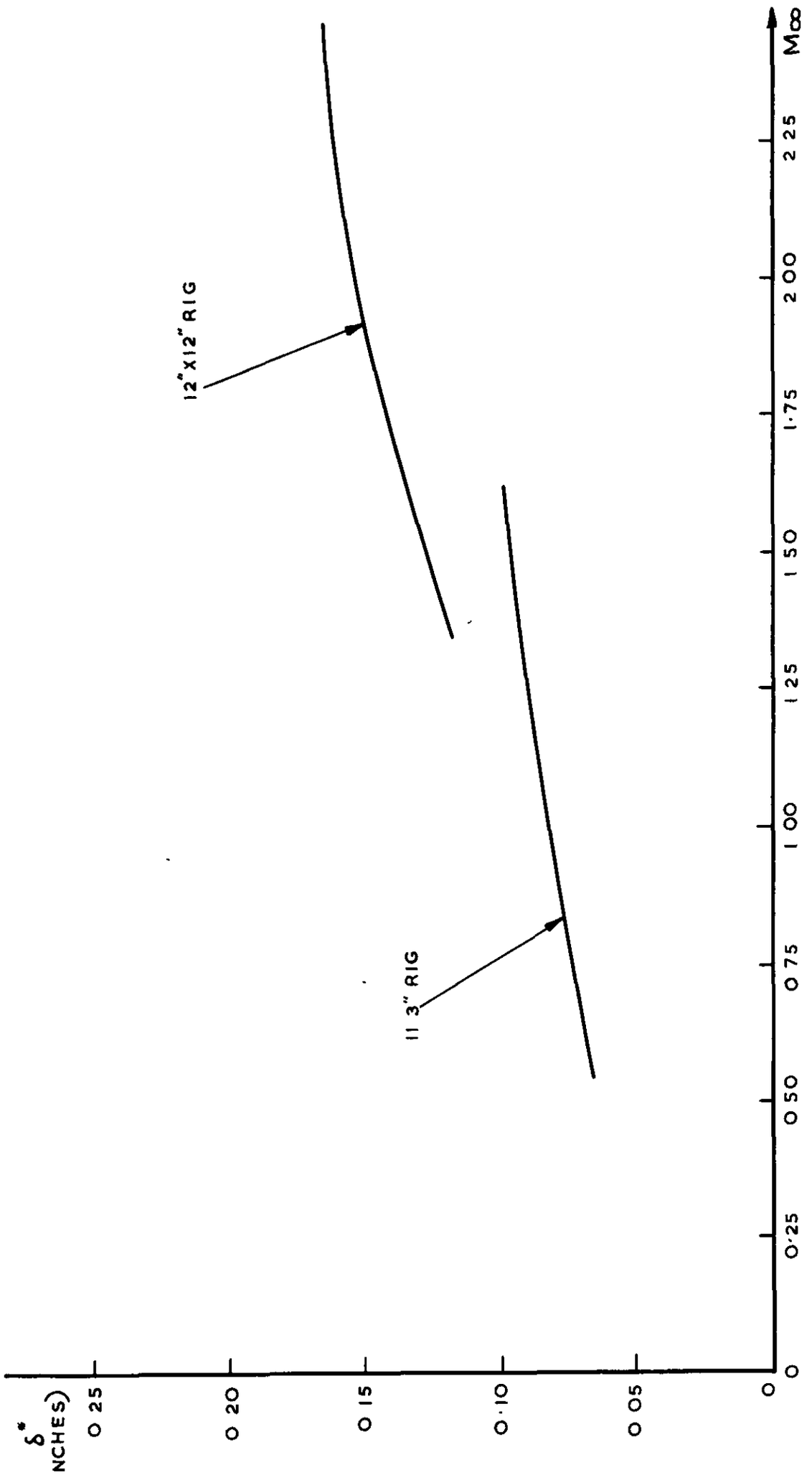

ESTIMATED VARIATION OF δ^* WITH M_∞.

FIG. 32

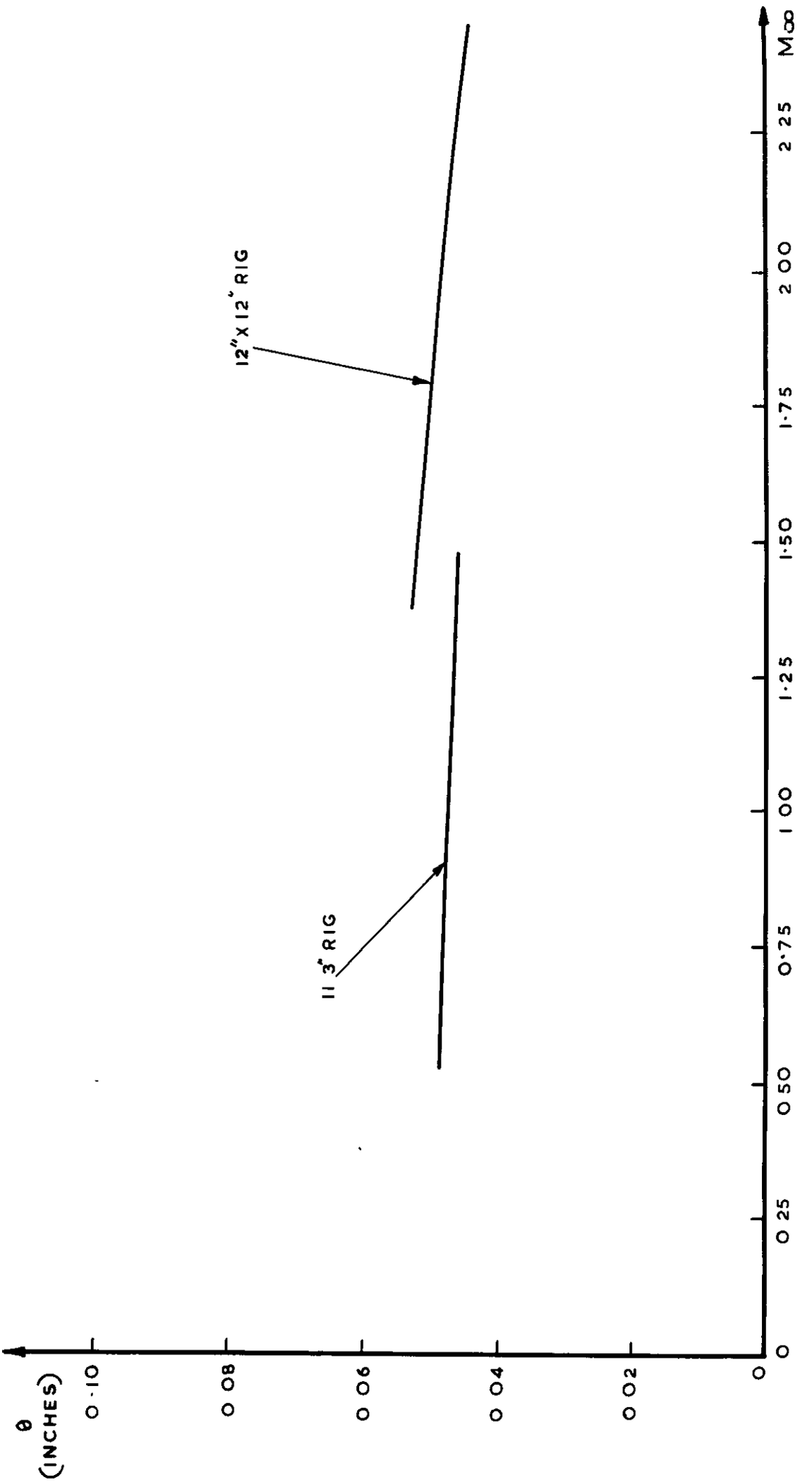

ESTIMATED VARIATION OF θ WITH M_∞.

A.R.C. C.P. No.892
February, 1964
Roberts, J. B. and Golesworthy, G. T.

621-225.1:533.691.18.093:
533.6.013.12

AN EXPERIMENTAL INVESTIGATION OF THE INFLUENCE OF BASE BLEED ON THE BASE DRAG OF VARIOUS PROPELLING NOZZLE CONFIGURATIONS

Various propelling nozzle configurations with all-internal expansion were tested in external flow over the range of Mach Number 0·7 to 2·2, in order to determine the effect of base bleed (i.e. the injection of low energy secondary air) on base pressure. An 'overall efficiency' is defined, which enables the effectiveness of base bleed, as a means of reducing the base drag, to be assessed. The results indicate that with supersonic external flow base bleed generally tends to raise the level of base pressure, but no improvement in the overall efficiency is obtained. At subsonic external speeds, the secondary air has a negligible effect on base pressure.

A.R.C. C.P. No.892
February, 1964
Roberts, J. B. and Golesworthy, G. T.

621-225.1:533.691.18.093:
533.6.013.12

AN EXPERIMENTAL INVESTIGATION OF THE INFLUENCE OF BASE BLEED ON THE BASE DRAG OF VARIOUS PROPELLING NOZZLE CONFIGURATIONS

Various propelling nozzle configurations with all-internal expansion were tested in external flow over the range of Mach Number 0·7 to 2·2, in order to determine the effect of base bleed (i.e. the injection of low energy secondary air) on base pressure. An 'overall efficiency' is defined, which enables the effectiveness of base bleed, as a means of reducing the base drag, to be assessed. The results indicate that with supersonic external flow base bleed generally tends to raise the level of base pressure, but no improvement in the overall efficiency is obtained. At subsonic external speeds, the secondary air has a negligible effect on base pressure.

A.R.C. C.P. No.892
February, 1964
Roberts, J. B. and Golesworthy, G. T.

621-225.1:533.691.18.093:
533.6.013.12

AN EXPERIMENTAL INVESTIGATION OF THE INFLUENCE OF BASE BLEED ON THE BASE DRAG OF VARIOUS PROPELLING NOZZLE CONFIGURATIONS

Various propelling nozzle configurations with all-internal expansion were tested in external flow over the range of Mach Number 0·7 to 2·2, in order to determine the effect of base bleed (i.e. the injection of low energy secondary air) on base pressure. An 'overall efficiency' is defined which enables the effectiveness of base bleed, as a means of reducing the base drag, to be assessed. The results indicate that with supersonic external flow base bleed generally tends to raise the level of base pressure but no improvement in the overall efficiency is obtained. At subsonic external speeds, the secondary air has a negligible effect on base pressure.

DETACHABLE ABSTRACT CARDS

Printed and published by

HER MAJESTY'S STATIONERY OFFICE

To be purchased from
49 High Holborn, London W C 1
423 Oxford Street, London W 1
13A Castle Street, Edinburgh 2
109 St Mary Street, Cardiff
Brazennose Street, Manchester 2
50 Fairfax Street, Bristol 1
35 Smallbrook, Ringway, Birmingham 5
80 Chichester Street, Belfast 1
or through any bookseller

Printed in England

S.O. Code No 23-9016-92